Draft version May 6, 2020
Typeset using LaTeX default style in AASTeX63

Galaxy And Mass Assembly: A Comparison between Galaxy-Galaxy Lens Searches in KiDS/GAMA.

Shawn Knabel,[1] Rebecca L. Steele,[1] Benne W. Holwerda,[1] Joanna S. Bridge,[1] Alice Jacques,[1] Andrew M. Hopkins,[2] Stephen P. Bamford,[3] Michael J. I. Brown,[4] Sarah Brough,[5] Lee Kelvin,[6] and Maciej Bilicki[7]

[1] *Department of Physics and Astronomy, 102 Natural Science Building, University of Louisville, Louisville KY 40292, USA*
[2] *Australian Astronomical Optics, Macquarie University, 105 Delhi Rd, North Ryde, NSW 2113, Australia*
[3] *School of Physics & Astronomy, University of Nottingham, University Park, Nottingham, NG7 2RD, UK*
[4] *School of Physics & Astronomy, Monash University, Clayton, VIC 3800, Australia*
[5] *School of Physics, University of New South Wales, NSW 2052, Australia*
[6] *Department of Astrophysical Sciences, Princeton University, 4 Ivy Lane, Princeton, NJ 08544, USA*
[7] *Center for Theoretical Physics, Polish Academy of Sciences, Warsaw, Poland*

Submitted to AJ

ABSTRACT

Strong gravitational lenses are a rare and instructive type of astronomical object. Identification has long relied on serendipity, but different strategies –such as mixed spectroscopy of multiple galaxies along the line of sight, machine learning algorithms, and citizen science– have been employed to identify these objects as new imaging surveys become available.

We report on the comparison between spectroscopic, machine learning, and citizen science identification of galaxy-galaxy lens candidates from independently constructed lens catalogs in the common survey area of the equatorial fields of the Galaxy and Mass Assembly (GAMA) survey. In these, we have the opportunity to compare high-completeness spectroscopic identifications against high-fidelity imaging from the Kilo Degree Survey (KiDS) used for both machine learning and citizen science lens searches.

We find that the three methods – spectroscopy, machine learning, and citizen science – identify 47, 47 and 36 candidates respectively in the 180 square degrees surveyed. These identifications barely overlap, with only two identified by both citizen science and machine learning. We have traced this discrepancy to inherent differences in the selection functions of each of the three methods, either within their parent samples (i.e. citizen science focuses on low-redshift) or inherent to the method (i.e. machine learning prefers well-separated arc and lens while spectroscopy requires the arc to lie within the fiber). These differences manifest as separate samples in lens mass and redshift. The combined sample implies a sky-density of ~ 0.72/sq degree and can serve as a training set spanning a wider mass-redshift space. For future searches a combined approach would result in a more complete sample of galaxy-galaxy lenses.

Keywords: Strong gravitational lensing, Galaxy dark matter halos, Redshift surveys, Giant elliptical galaxies

1. INTRODUCTION

Elliptical galaxies' structure, kinematics, and formation histories are a compelling test of the Cold Dark Matter (ΛCDM) paradigm as they are the end-product of galaxy formation (De Lucia et al. 2006). Strong gravitational lenses appear in every respect to be just like other elliptical galaxies, so results of their study can therefore be generalized to all spheroidal galaxies in the observed mass range (Auger et al. 2009a). These lensing systems provide a highly accurate measurement of the *total* mass, and therefore the dark matter content, in these elliptical galaxies that compares well with current galaxy evolution models and assumptions (Shu et al. 2014, and reference therein). To date, gravitational lenses have proven General Relativity to be correct with high accuracy over galaxy-wide scales (Collett et al. 2018)

and may provide an excellent test case for other theories of gravity, such as the Emergent Gravity recently proposed by Verlinde (2016), through a combination of lensing and kinematic measurements (see Tortora et al. 2017).

Gravitational lensing has been a powerful technique to measure the masses of the *most massive* elliptical galaxies (Gavazzi et al. 2007; **?**), constraining their Fundamental Plane (Bolton et al. 2008), the stellar population's mass-to-light ratio, and thus their initial mass function (IMF; Auger et al. 2009a; Hopkins 2018). The observational drive is now to measure their mass content throughout the spheroidal galaxy mass function (**?**), explore the Fundamental Plane in different environments (Treu et al. 2009), constrain the stellar mass-to-light ratio in nearby ellipticals (Treu et al. 2006; Collier et al. 2018a,b), discover dark matter substructure in known strong galaxy lens cases (Cyr-Racine et al. 2018), and independently measure H_0 through time-delay cosmography (e.g. H0LiCOW, Chen et al. 2019). These observational studies need larger samples of lenses.

Thus far, lensing arcs have predominantly been identified in *massive* ($> 10^{11} M_\odot$) lens systems thanks to selection biases: SDSS spectroscopic targets are volume-weighted to greater mass, and visual identification favors well-separated arc and lens (Shu et al. 2014). With the GAMA spectroscopy-selected sample (Holwerda et al. 2015), a much greater range in lens masses is now available. However, the drive for much larger samples has led to increased searches using machine learning to constrain ΛCDM in detail (Petrillo et al. 2017, 2018; **?**; Speagle et al. 2019; Huang et al. 2019; Jacobs et al. 2019).

The success and completeness of the different identification techniques are difficult to test against one another. This has motivated our study here that benefits from three independent identifications – spectroscopic, machine learning and citizen science – on the same target fields. Our aim is to compare all three techniques to map out an optimal path for future searches.

2. IDENTIFYING STRONG GALAXY-GALAXY LENSES

The principal selection technique for galaxy-galaxy lenses has been the identification of double spectral profiles in a single aperture based spectrum (blended spectra, see Bolton et al. 2004; Holwerda et al. 2015, Steele et al. *in prep.*). Searches for blended spectra in the Sloan Digital Sky Survey (SDSS) have been highly successful in identifying strong-lens galaxies by identifying spectra containing both a low-redshift passive galaxy and emission lines from a much higher-redshift lensed source. In order to confirm such sources as true lensing systems, one requires significantly higher spatial resolution imaging than the SDSS can provide.

85 cases of strong lenses have already been confirmed with Hubble Space Telescope (HST) imaging through the SLACS[1] survey (Treu et al. 2006; Koopmans et al. 2006; Gavazzi et al. 2007; **?**, 2008; Bolton et al. 2008; Treu et al. 2009; Auger et al. 2009a). The SLACS survey was efficient in finding these rare strong lensing objects: approximately 50% of the blended spectra (with a dispersion estimate of the Einstein radius) targeted were confirmed with HST observations, and its success has expanded into the BOSS survey and higher redshifts ($0.4 < z < 0.7$, Brownstein et al. 2012).

However, due to the depth and completeness limitations of SDSS spectroscopy, typically only massive foreground galaxy lenses can be identified ($10^{11} - 10^{12} M_\odot$) at intermediate redshifts ($z = 0.15 - 1$). If the lensing arc does not intersect with the SDSS aperture, there will not be sufficient flux from the source galaxy to identify it as a lens. In addition, the SLACS survey (SLACS & S4TM, Shu et al. 2015) imposed a redshift cut of z ¿ 0.15 for the majority of the lens candidates that were selected from the LRG sample. **According to Hilbert et al. (2008) the lensing cross section drops rapidly below z 0.5, so naturally there are fewer lenses at lower redshifts. However, Sonnenfeld et al. (2015), referencing Arneson et al. (2012) and ?, claims that "the Einstein radius seems to be the main quantity determining the detection probability. Of the two terms in the selection function, the Einstein radius selection is the dominant one while the lensing cross section correction has little effect on the results of our analysis." Einstein radius as a function of the mass and redshift arrangement, with higher mass and closer lenses resulting in larger Einstein radii, is biased by the size of the survey's spectroscopic aperture. Only with a significant expansion of the lensing sample can the effects of evolution and stellar mass be decoupled (e.g., Treu et al. 2006). In the following calculations we adopt a cosmological model with $h_0 = 0.738$, where $h_0 = \frac{H_0}{100}\ km\ Mpc^{-1}s^{-1}$ indicated in Riess et al. (2011).**

[1] Survey of Lenses with the Advanced Camera for Surveys

2.1. *GAMA Spectroscopic Identification*

The Galaxy and Mass Assembly survey (GAMA; Driver et al. 2009, 2011) is a multi-wavelength survey built around a deep and highly complete redshift survey of five fields with the Anglo-Australian Telescope. GAMA has three major advantages over SDSS in the identification of blended spectra: (1) the spectroscopic limiting depth is 2 magnitudes deeper ($m_r < 19.8$ mag.), (2) the completeness is close to 98% (Liske et al. 2015), and (3) the AUTOZ redshift algorithm easily identifies spectra with signal from two different redshifts (Baldry et al. 2014). In the GAMA survey, Holwerda et al. (2015) identified !!!!!!! 104 strong lensing candidates from their blended spectra. This spectroscopically identified sample is dominated by lower-mass spheroidal galaxies and higher-redshift galaxies (Steele et al. *in prep.*).

These GAMA strong lens candidates from (Holwerda et al. 2015, Steele et al. *in prep.*) extend the stellar mass range and provide a medium-redshift observation in between the SLACS, S4TM, and BELLS samples. Chan et al. (2016) verified some 70% of these spectroscopically identified lenses using deep Subaru imaging.

As mentioned above, the spectroscopic approach is intrinsically limited by the aperture of the spectroscopy: if the lensed features fall outside it, the signal of the lensed (source) galaxy will be weak (Sonnenfeld et al. 2015; Arneson et al. 2012). As a result of this, GAMA spectroscopy structurally misses lower redshift and higher mass lenses. GAMA has improved the spectroscopic identification of lower mass strong lenses, but a much larger sample of lower redshift ($z < 0.1$) lenses is needed to constrain mass-to-light ratios in ellipticals.

2.2. *Beyond Spectroscopic Identification of Lenses*

2.2.1. *Machine Learning Identification of Lenses*

Machine learning is gaining popularity as a method for identifying galaxy-galaxy lenses, e.g. in Subaru Hyper-Supreme Cam (Speagle et al. 2019), DECAM (Huang et al. 2019), and Dark Energy Survey data (Jacobs et al. 2019). Petrillo et al. (2017) and Petrillo et al. (2018) introduced and developed a machine learning technique to visually identify strong lenses by training the neural networks to recognize the characteristic arcs that appear next to a lensing elliptical galaxy. Their selection process included a follow-up visual inspection of each candidate by seven members of the team, which provided a score for each candidate between 0 (reflecting low confidence) and 70 (reflecting high confidence). This new identification method resulted in the 1300 candidate galaxy-galaxy Lenses in the Kilo-Degree Survey (LinKS) sample (KiDS; de Jong et al. 2013, 2015, 2017; Kuijken et al. 2019), which overlaps with 100% of the equatorial fields of the GAMA survey (fields G09, G12, and G15). These identifications by Petrillo et al. (2018) have shown that there are many more strong lenses to be found in the same survey area using identification methods other than spectroscopic. This approach has succeeded in finding more candidate strong lenses similar to the simulated massive elliptical galaxies on which the neural network was trained.

2.2.2. *Citizen Science Identification of Lenses*

GalaxyZoo (Lintott et al. 2008) has classified KiDS postage stamps of galaxies on the same area that corresponds to the GAMA+KiDS survey overlapF (Kelvin et al. *in prep*, Holwerda et al. 2019) and using a question tree design presented below in Figure 1. It leads participants through a series of questions that (given the object is a galaxy) will arrive at a question that prompts them to identify any number of the following "odd features" in the image: "None", "Ring", "Lens or arc", "Dust lane", "Irregular", "Other", and "Overlapping". With the voting completed on the GAMA+KiDS equatorial fields, we can now analyze and compare the results of the citizen science approach to the spectroscopic and machine learning ones.

With three independent techniques to identify strong gravitational lenses in the same three fields, we have an opportunity to test how well different identification techniques can be calibrated against one another, discover implicit selection effects in each, and approximate the on-sky density of strong galaxy lenses.

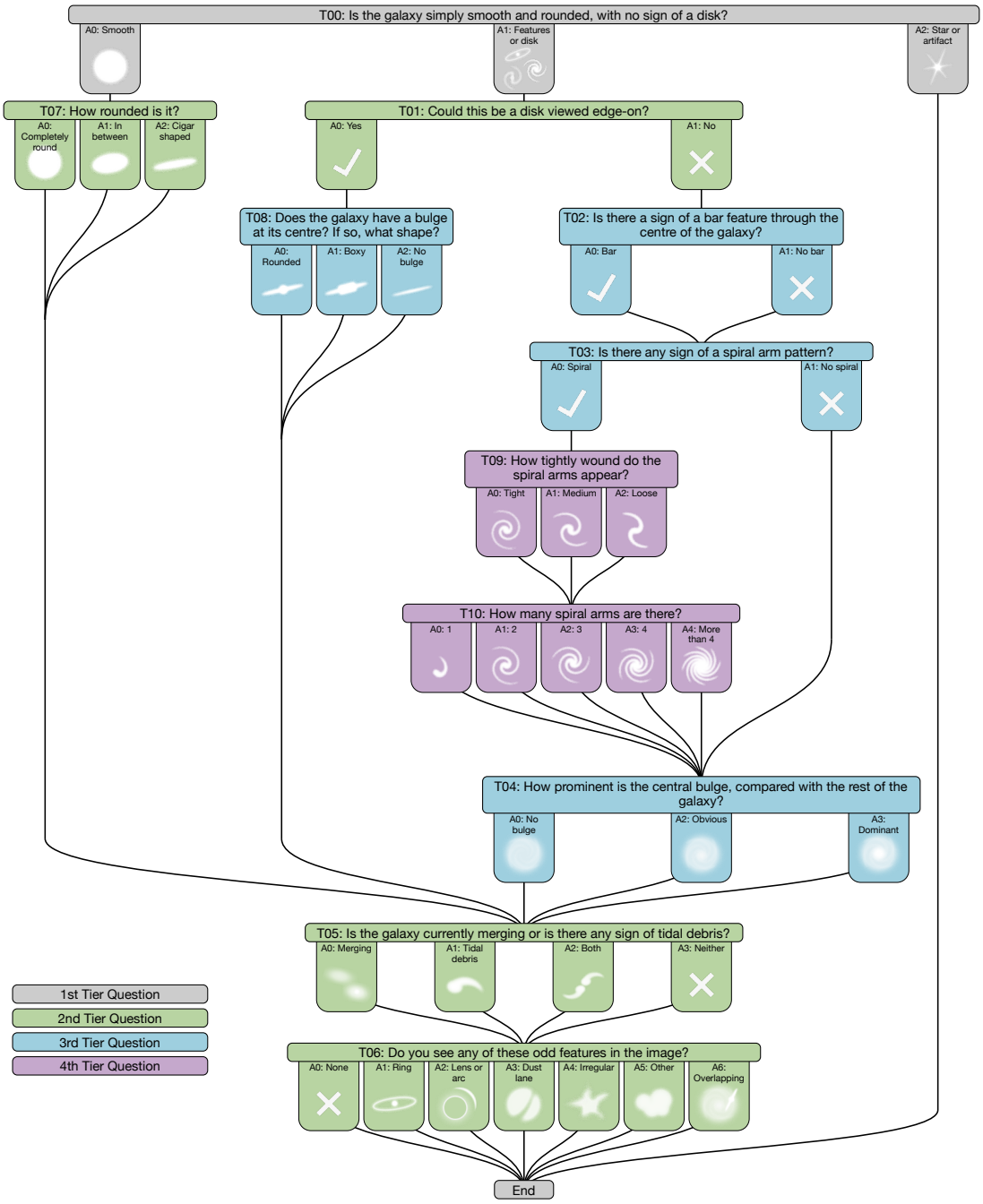

Figure 1. The question tree employed by GalaxyZoo citizen science, which volunteer participants use to classify images from the Kilo-Degree Survey (KiDS). 2nd Tier Question T06 prompts participants to identify "odd features," of which an option is "Lens or arc." Participants can choose more than one option in T06. We used results from this question to determine the final cut for our GalaxyZoo selection.

3. DATA AND OBSERVATIONS

In order to obtain a valid comparison of the three techniques, the catalogs of candidate lenses obtained by GAMA blended spectra (Holwerda et al. 2015), LinKS machine learning (Petrillo et al. 2018), and GalaxyZoo citizen science (Kelvin et al. *in prep.*) were cut to represent only those candidates identified within the equatorial GAMA fields G09, G12, and G15, which is the area of overlap between GAMA and KiDS. We show the presence of candidates identified by each method in each of those fields in Figure 2. This cut resulted in usable catalogs consisting of 85 spectroscopically-identified lens candidates, 421 candidates identified by LinKS machine learning, and a misleading total of 12934 GalaxyZoo candidates with "Lens or arc" scores of 0 or higher. Further cuts (see below in Sections 3.1,**??**, and 3.2) to the catalogs were then made to account for false positives in each of the samples.

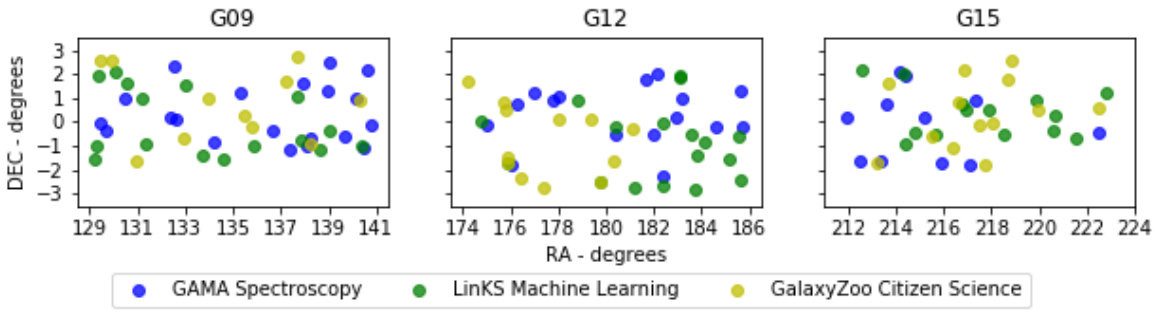

Figure 2. The three GAMA/KiDS fields (G09, G12 and G15) within which all three lensing identification techniques are available. GAMA spectroscopic, KiDS GalaxyZoo citizen science and KiDS machine learning identifications of galaxy-galaxy lens systems are identified in all three fields.

Stellar mass estimates and redshifts for each candidate were taken from the GAMA MAGPHYS catalog (Wright et al. 2018) and checked with WISE masses (Cluver et al. 2014) from GAMA DR2/3 (Liske et al. 2015; Baldry et al. 2018). Candidates were matched between independent catalogs by GAMA ID, except for the LinKS sample, which was matched based on RA and DEC.

3.1. *GAMA Blended Spectra and LinKS Machine Learning Catalogs*

The lens candidate sample provided by Holwerda et al. (2015) is based on spectral match, and therefore does not include a subjective follow-up visual inspection. However, in order to attain a more pure sample for consideration here, we selected candidates with a minimum difference of $\Delta z > 0.1$ between the redshift of the passive galaxy spectral match and an emission line galaxy match at higher redshift. This selection is shown in Figure 3 in comparison to Grade-A SLACS lenses from Auger et al. (2009b). Note that first redshift matches for GAMA spectroscopy do not necessarily correspond to the closer of the two galaxies. In all cases, the closer of the two is the PG, even if the first spectral match was to the ELG. The result is 47 candidates identified by GAMA spectroscopy, **All following mentions of the GAMA spectroscopy sample refer to this reduced selection of candidates unless otherwise specified.**

The LinKS machine learning catalog of 421 candidates obtained from Petrillo et al. (2018) included all those objects whose visual inspection score was greater than 0. In order to compare only the highest quality candidates, a score threshold of > 17 was taken from Petrillo et al. (2017) as representing higher quality candidates. This reduced the LinKS machine learning catalog to 47. **All following mentions of the LinKS machine learning sample refer to this reduced selection of candidates unless otherwise specified.**

3.2. *Citizen Science (GalaxyZoo) catalog*

GalaxyZoo presented the most variables to consider when analyzing its reliability as a method for identifying strong lenses. The percentage of votes for lensing features in each candidate is taken to be a subjective score given in a similar manner to the LinKS machine learning catalog. Since the program was not designed specifically to identify

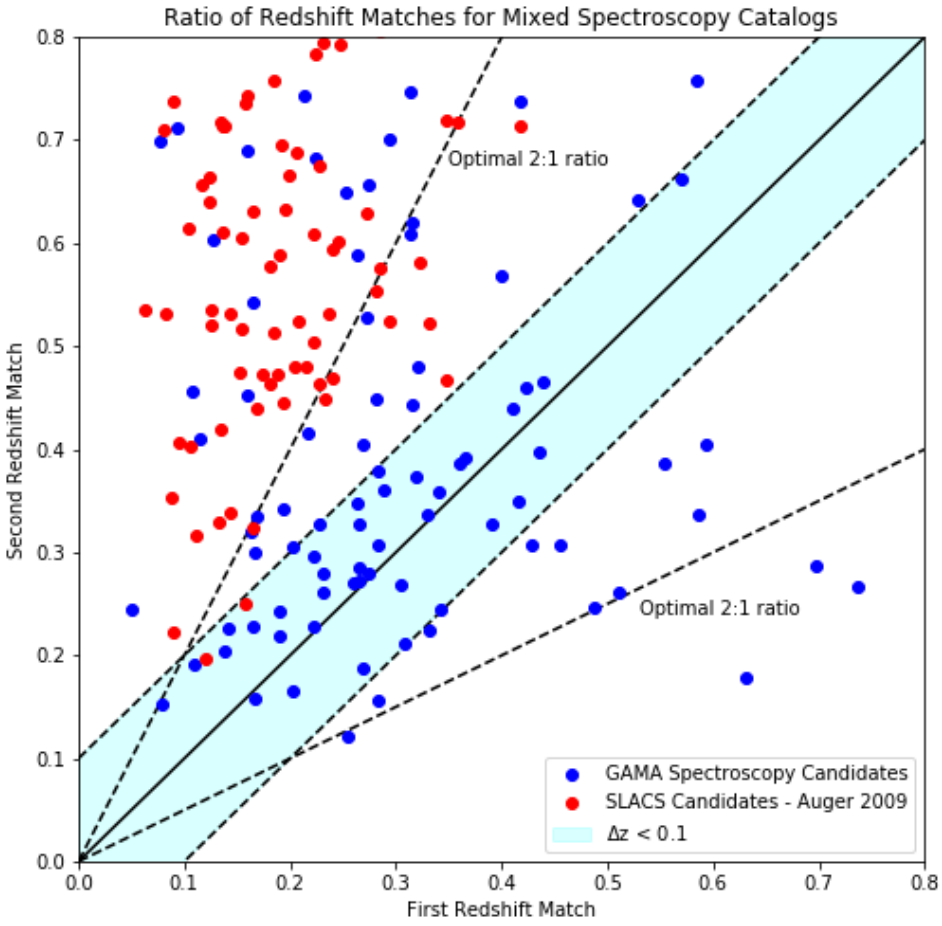

Figure 3. Selection of GAMA Spectroscopy Candidates based on redshift difference.

only lenses, each candidate's score must also be considered relative to scores of other choices within the same question level. For each candidate in question, other "odd features" could potentially pull votes away from the "Lens or arc" classification.

Selection votes could be distributed unpredictably across the seven options, so we took a multi-faceted selection cutoff informed by visual comparison of candidates of a range of "Lens or arc" scores, examples of which are shown in Figure 5, as well as comparing them with LinKS machine learning candidates, in addition to analyzing ratios of "Lens or arc" scores to the scores given to each of the other six "odd feature" options, which we demonstrate in Figure 6. We considered doubt in the participants' visual inspection to bias the selection toward "None" if features did not seem "odd" enough, so we added an additional provision to our cutoff. Our final selection considered only those candidates with the following characteristics:

1. "Lens or Arc" score was greater than all other "odd feature" options' scores with the exception of "None".

2. "Lens or Arc" score was greater than half the score given to "None".

3. "Lens or Arc" score was greater than 30 percent.

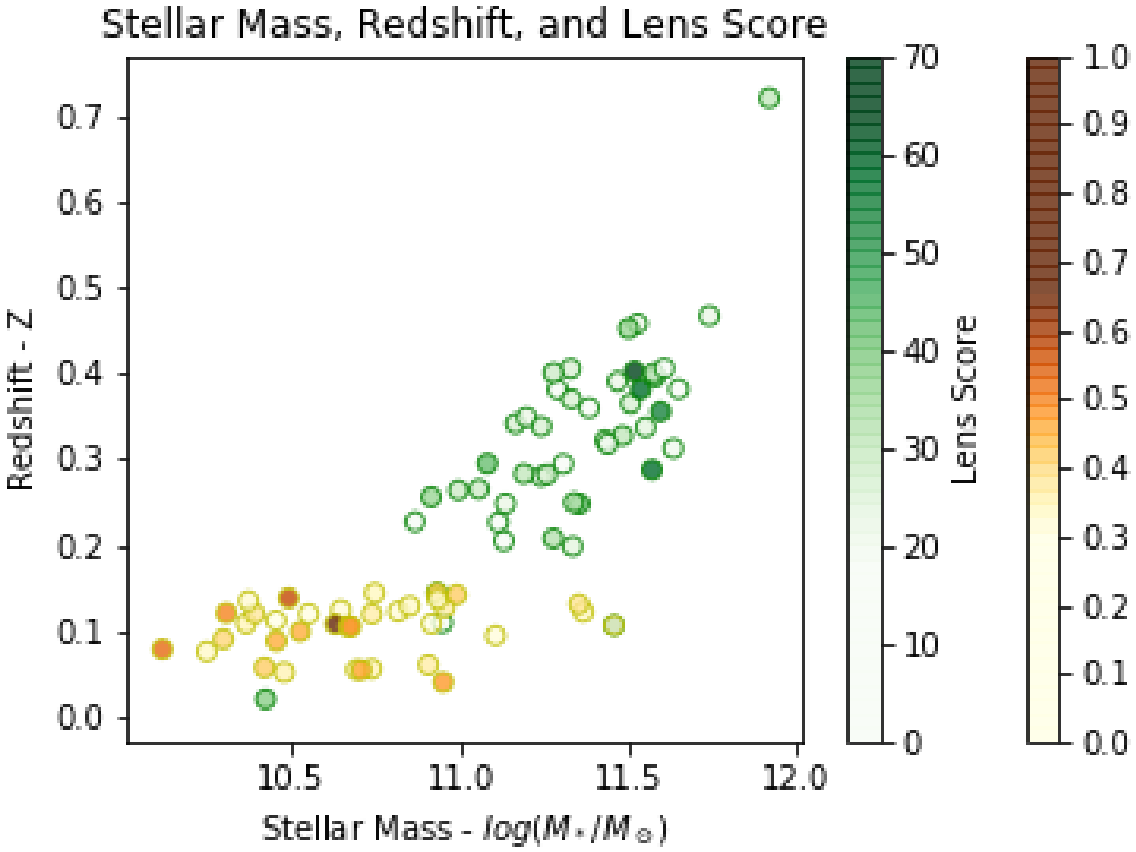

Figure 4. Green markers show the stellar mass and redshift of strong lens candidates identified by LinKS machine learning from **?**. LinKS lens score reflected by the green color bar refers to the authors' visual inspection and scoring of lenses on a scale of 0-70, with higher numbers reflecting higher confidence. High-scoring objects occur throughout the mass and redshift range, with the highest scoring above $\log(M_*/M_\odot) = 11.4$. Yellow-to-brown markers indicate the stellar mass and redshift of our final selection of GalaxyZoo candidates (Kelvin et al *in prep*). GalaxyZoo lens score shown by the yellow-to-brown color bar refers to the fractional score out of 1 indicating the fraction of votes for "Lens or arc" for each candidate, with higher numbers reflecting higher confidence. High-scoring objects occur throughout the mass and redshift range.

In addition, only those candidates whose estimated Einstein radius (Section !!! for details) is larger than the point spread function (PSF) for KiDS imaging (0.65 arcsec) were included in the final selection. This selection, based on the capabilities of the instrument, removes several high-scoring candidates from consideration, as shown in Figure 7.

This final cut reduced the GalaxyZoo citizen science catalog to 36 candidates (listed in Table 3 in the Appendix) of roughly comparable reliability to the other two techniques, according to our own visual inspection of various scoring lenses. These candidates fell mostly within a mass range of !!!! $\log(M_*/M_\odot) = 9.5 - 11$ at redshifts below $z = 0.15$, which was a redshift restriction imposed by the GalaxyZoo team in the pre-selection of images to be classified by participants. **All following mentions of the GalaxyZoo citizen science sample refer to this reduced selection of candidates unless otherwise specified.**

3.3. *Einstein Radius Estimation*

Limited by the exclusion of velocity dispersion measurements of the GAMA/KiDS fields, we approximate the lens galaxy as a point-mass system with there lens and source positioned along the same line of sight, where the Einstein radius (θ_E) is given by

$$\theta_E = (\frac{M}{10^{11.09} M_\odot})^{1/2} (\frac{D_{LS}}{D_L D_S} Mpc)^{1/2} arcsec$$

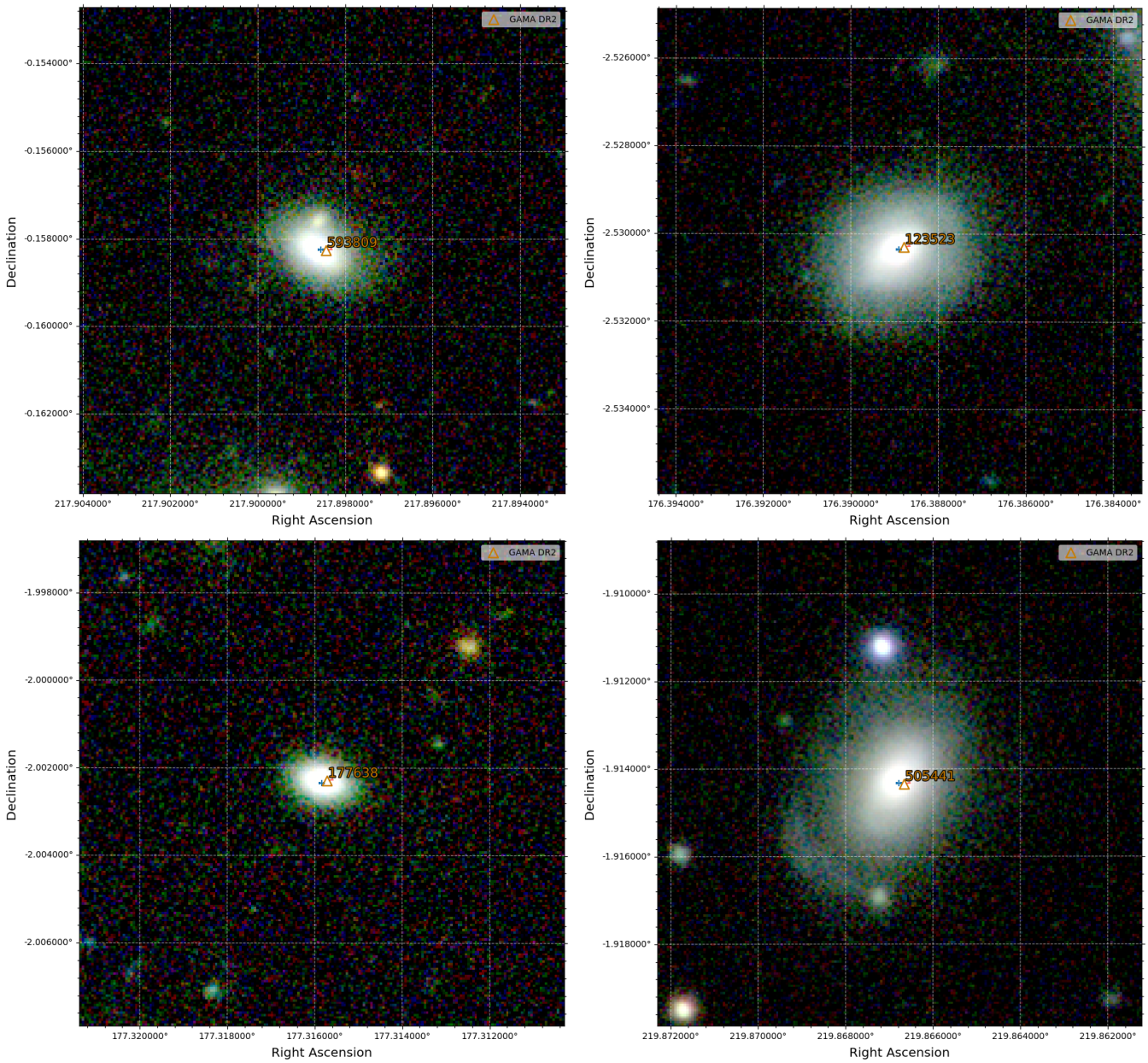

Figure 5. Examples of lens candidates identified by GalaxyZoo citizen science, taken from KiDS (*g-*, *r-*, and *i*-bands). G593809 (top left) represents a "Lens or arc" score of 10% of votes. G123523 (top right) represents a "Lens or arc" score of 20%. G177638 (bottom left) represents a "Lens or arc" score of 25%. G505441 (bottom right) represents a "Lens or arc" score of 30%. These are representative of the images that would be viewed by GalaxyZoo participants, as well as informing our final cutoff for the GalaxyZoo selection considered here.

where M is the total mass enclosed by the Einstein radius, D_{LS} is the distance from lens to source, D_L is the distance from observer to lens, and D_S is the distance from observer to source. Utilizing stellar mass measurements from the GAMA MagPhys catalog (Wright et al. 2018) and assuming dark matter fraction of f_{DM} 61% (average taken from Barnabè et al. (2011) assuming Chabrier IMF), we estimate the total mass. Only the GAMA spectroscopy candidates include source redshift measurements; for these candidates, D_{LS} and D_S are calculated from this redshift. For LinKS machine learning and GalaxyZoo citizen science candidates, the lens galaxy is assumed to be positioned approximately halfway between the observer and source. This is the distance at which the most prominent features should be observable. Calculations performed here are considered to be underestimates due to the conservative assumption of an average f_{DM} that is in reality mass-weighted Barnabè et al. (2011) and likely higher for several candidates.

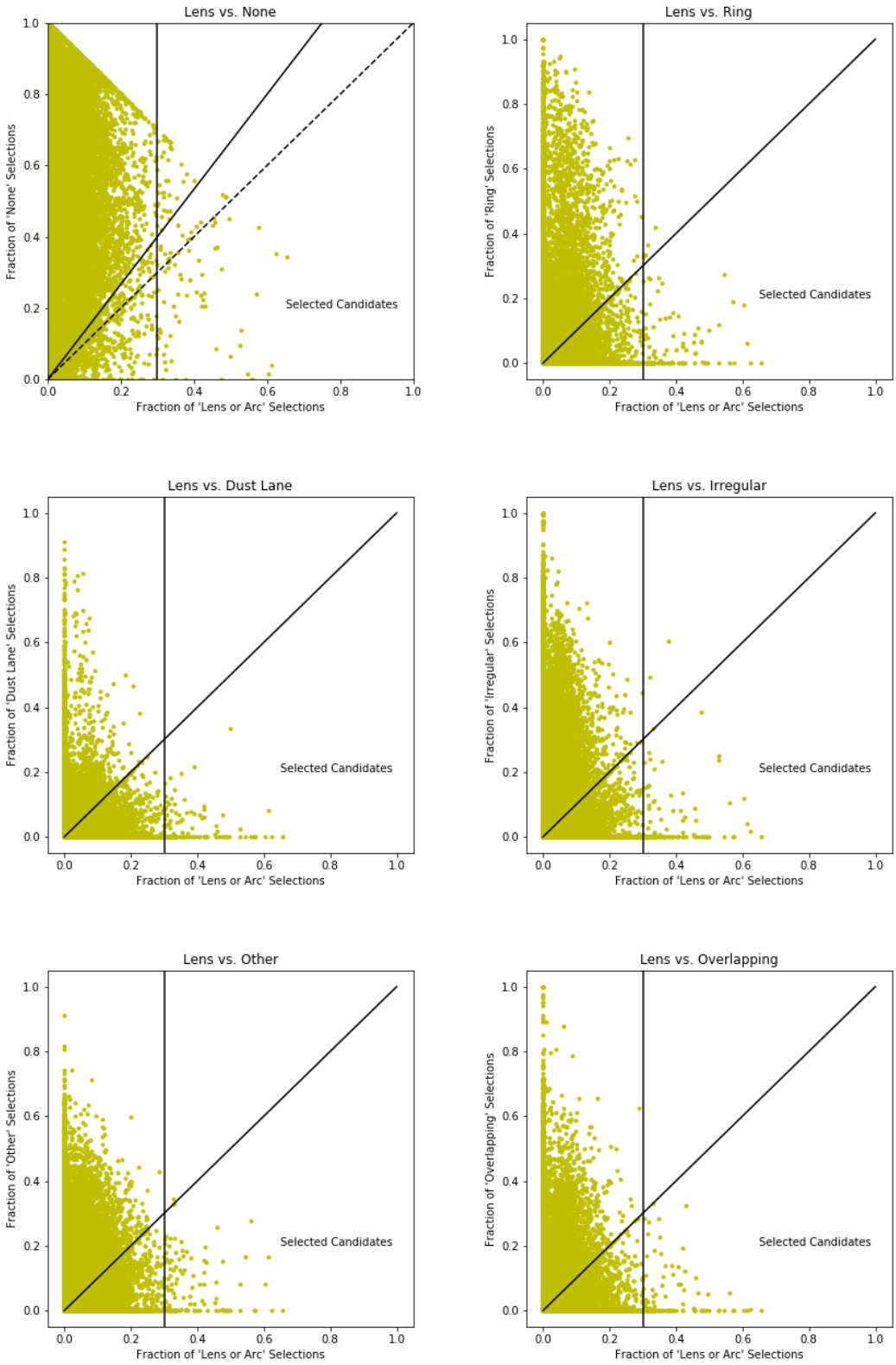

Figure 6. Ratios of the fraction of "Lens or arc" scores relative to the other six "odd features" options from GalaxyZoo Question Tree question T06, shown above in Figure 1. Solid lines indicate boundaries used in the final cut for the GalazyZoo selection. All points contained within the region to the right of the vertical line and below the diagonal line represent a candidate selected for our final GalaxyZoo sample.

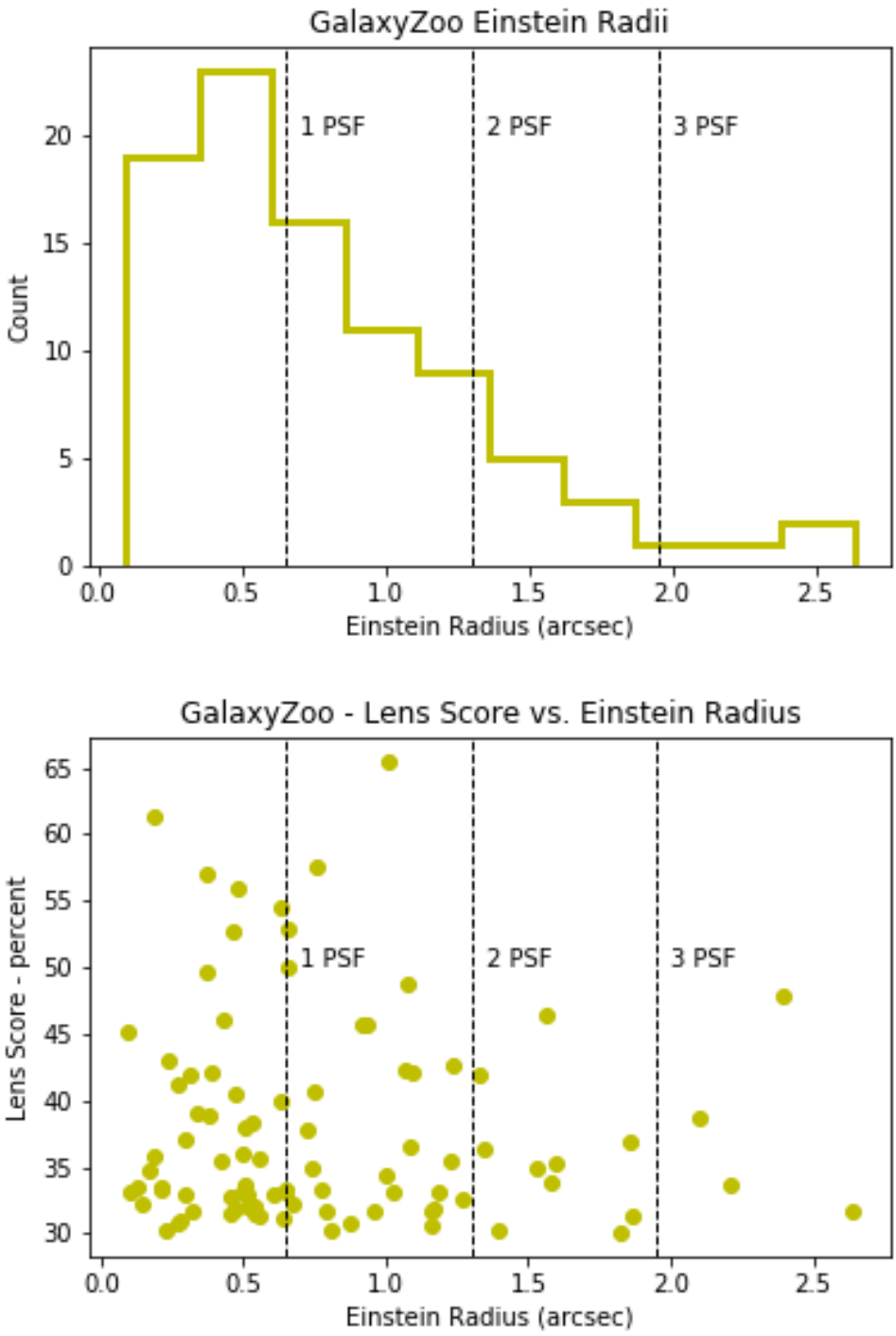

Figure 7. (Top) Histogram showing the distribution of Einstein radius estimates for GalaxyZoo citizen science candidates that pass the question tree portion of selection criteria. (Bottom) Vertical axis shows "Lens or arc" score as percentage of votes. Candidates with estimated Einstein radii lower than the KiDS PSF are considered poor candidates and are removed from the final sample. The high scoring GalaxyZoo objects in this removed subsample are good candidates for tidal features.

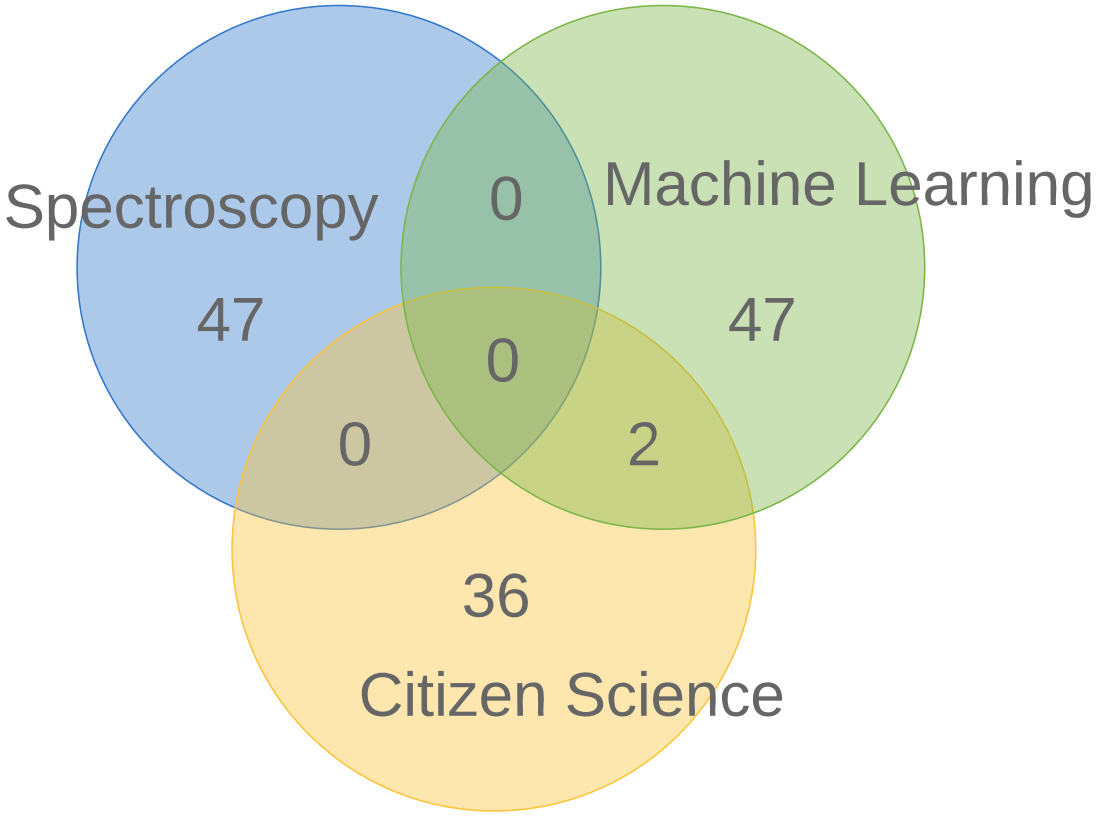

Figure 8. Venn diagram showing the number of lens candidates identified by each of the three methods following our final cuts. Overlapping regions indicate the number of lens candidates identified by both (or all three) candidates. The only overlaps occurred between LinKS machine learning and GalaxyZoo citizen science.

4. RESULTS

We found remarkably little overlap between catalogs of candidates obtained by the three methods. Our final cuts of the three catalogs included no candidate common to all three methods and only two candidates common to two methods, both of which were between LinKS machine learning and GalaxyZoo citizen science, as shown in Figure 8.

4.1. *Results of Einstein Radius Estimates*

The Einstein radius is a fundamental feature of a lensing system that determines to a large degree the probability of detection by any lens finding method (!!! Sonnenfeld, Arneson, etc.). The results of the estimates, displayed in Figures 9 and 13 show that the majority of GAMA spectroscopy candidates have Einstein radii smaller than or close to the 1-arcsecond GAMA spectroscopy aperture radius, as expected. The majority of candidates from the image-based machine learning and citizen science methods have characteristic Einstein radii close to or greater than 1 arcsecond, above the PSF where images of the lens galaxy and arc features can be distinctly separable. Reference θ_E estimates of SLACS (!!! Bolton08), S4TM (Shu et al. (2017)), and BELLS (!!! Brownstein11) grade-A lens candidates are shown in the bottom plot of Figure 9. The LinKS machine learning sample identified candidates with comparable Einstein radii to the SLACS sample (which was the guide for its training sample), and S4TM and BELLS can be seen to approach the

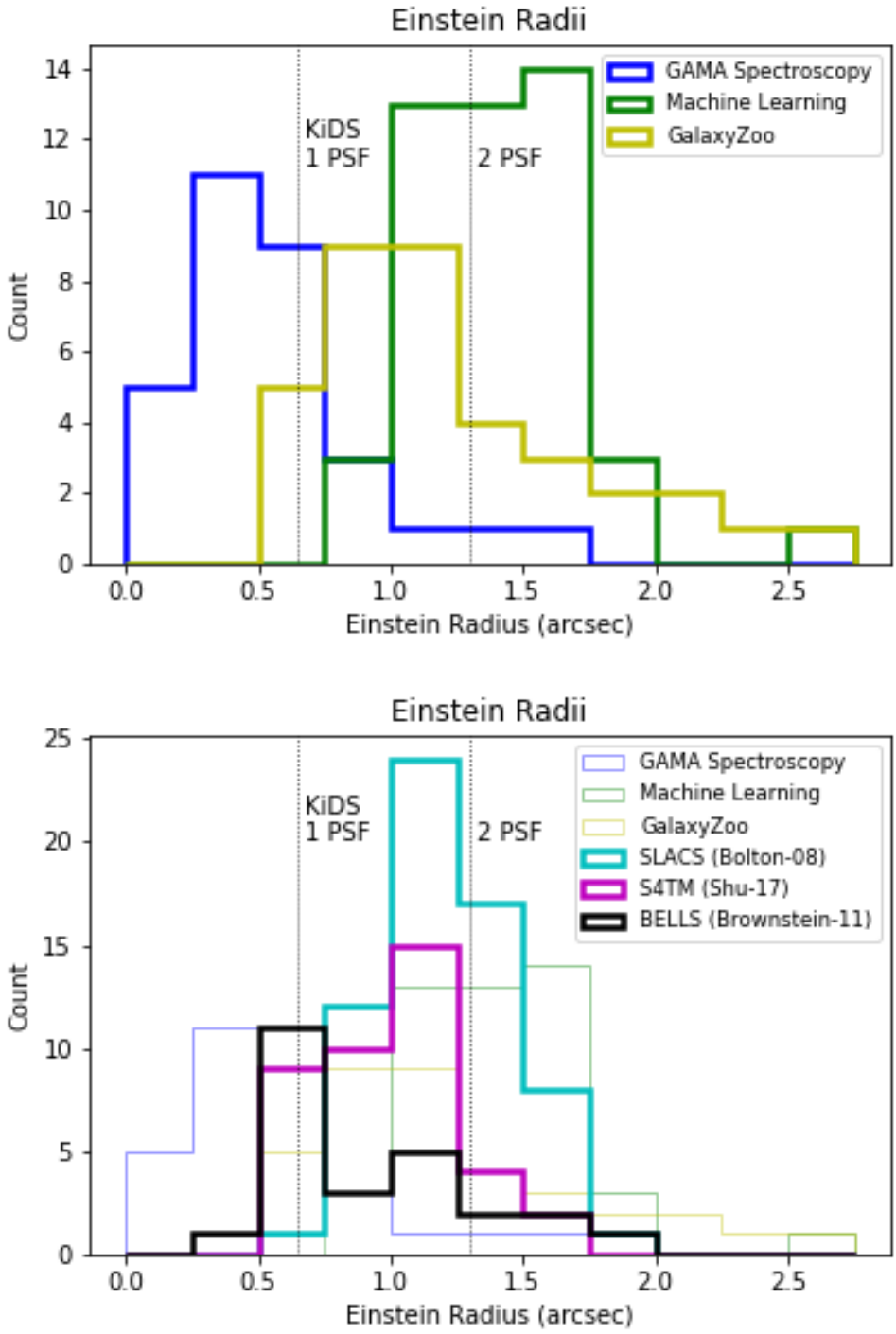

Figure 9. Einstein Radius Estimates EXPAND

smaller Einstein radii identified in GAMA spectroscopy. **GAMA spectroscopcially identified lenses extend to lower Einstein radii as GAMA selection suffers less from a mass bias thanks to the high completeness.**

4.2. *Stellar Mass and Redshift Space*

Analyzing the properties of each catalog in terms of the candidates' stellar mass and redshift, which we illustrate in Figure 10, we discovered that each method identified galaxies with a distinct range of redshifts and masses.

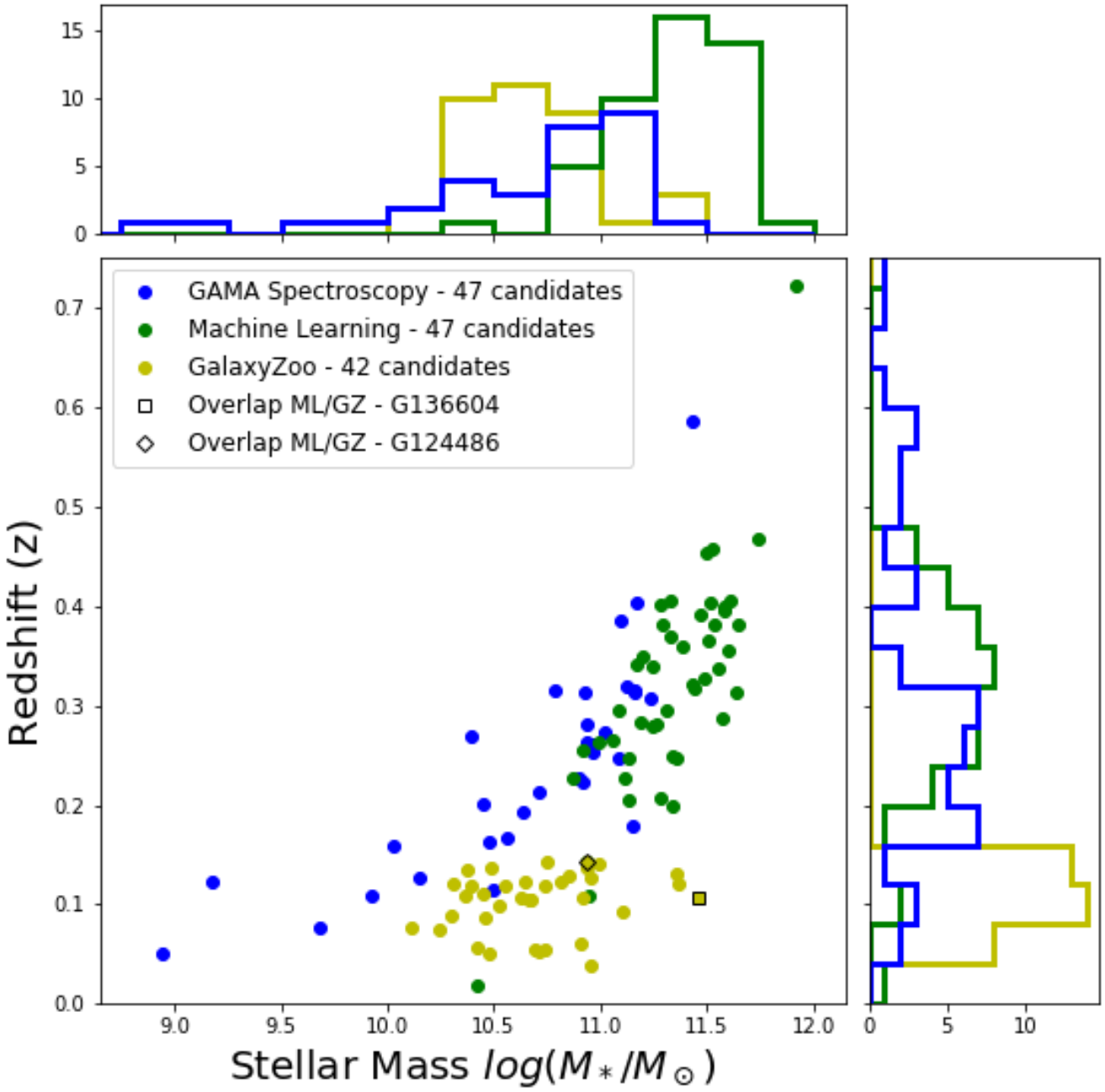

Figure 10. Distribution of lens candidates identified by each of the three methods in terms of each candidate's stellar mass and redshift. Histograms above and to the right of the scatter plot indicate the number of candidates identified by each method within specific ranges of stellar mass and redshift respectively. Each method's catalog occupies a unique range of both characteristics.

The candidates identified through GAMA spectroscopy tended to be found between $z \sim 0.1 - 0.4$ and with stellar masses between $\log(M_*/M_\odot) = 10.5 - 11.5$, with a few as low as $\log(M_*/M_\odot) = 9$. For each redshift in the range, there is a maximum total mass for which the Einstein radius fits in the spectroscopic aperture of the GAMA survey (angular diameter $= 2''$). This is lower than the SDSS maximum mass due to narrower fiber aperture (SDSS fiber aperture is $3''$). See Section 6.4 and Figure 12.

Those candidates identified through LinKS machine learning spanned a slightly higher redshift range and tended to be slightly more massive, mostly above $\log(M_*/M_\odot) \sim 11$. As Figure 4 shows, high scoring LinKS candidates can be

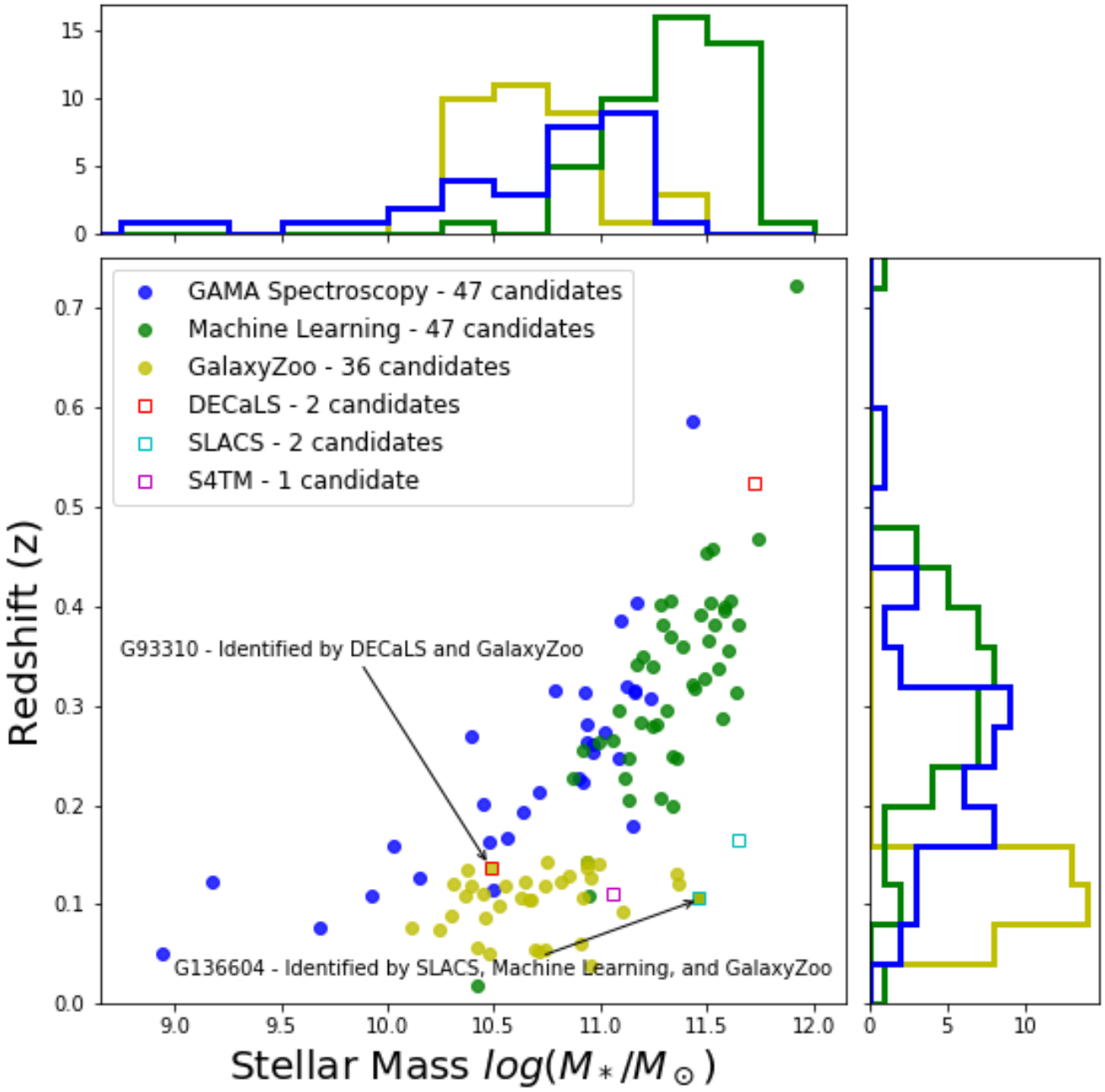

Figure 11. The data here is the same as in Figure 10 with the addition of five square markers indicating candidates previously identified by DECaLS (!!!cite), SLACS (!!! cite), and S4TM in the GAMA equatorial regions and which had a match in RA/DEC to the GAMA catalog. Two of these candidates were identified by GalaxyZoo citizen science, and one of those two was also identified by LinKS machine learning.

found throughout the redshift-mass range, with the highest scoring above $\log(M_*/M_\odot) = 11.4$. This is because the training set for the Petrillo et al. (2018) LinKS machine learning method is based on intermediate redshift massive galaxies that would have been identified in SDSS spectroscopy, i.e. the SLACS identified sample.

GalaxyZoo identified candidates definitively below the catalog's $z < 0.15$ cutoff, while finding candidate galaxies distributed in the mass range as the bulk of the spectroscopic candidates, $\log(M_*/M_\odot) = 10.0 - 11.0$.

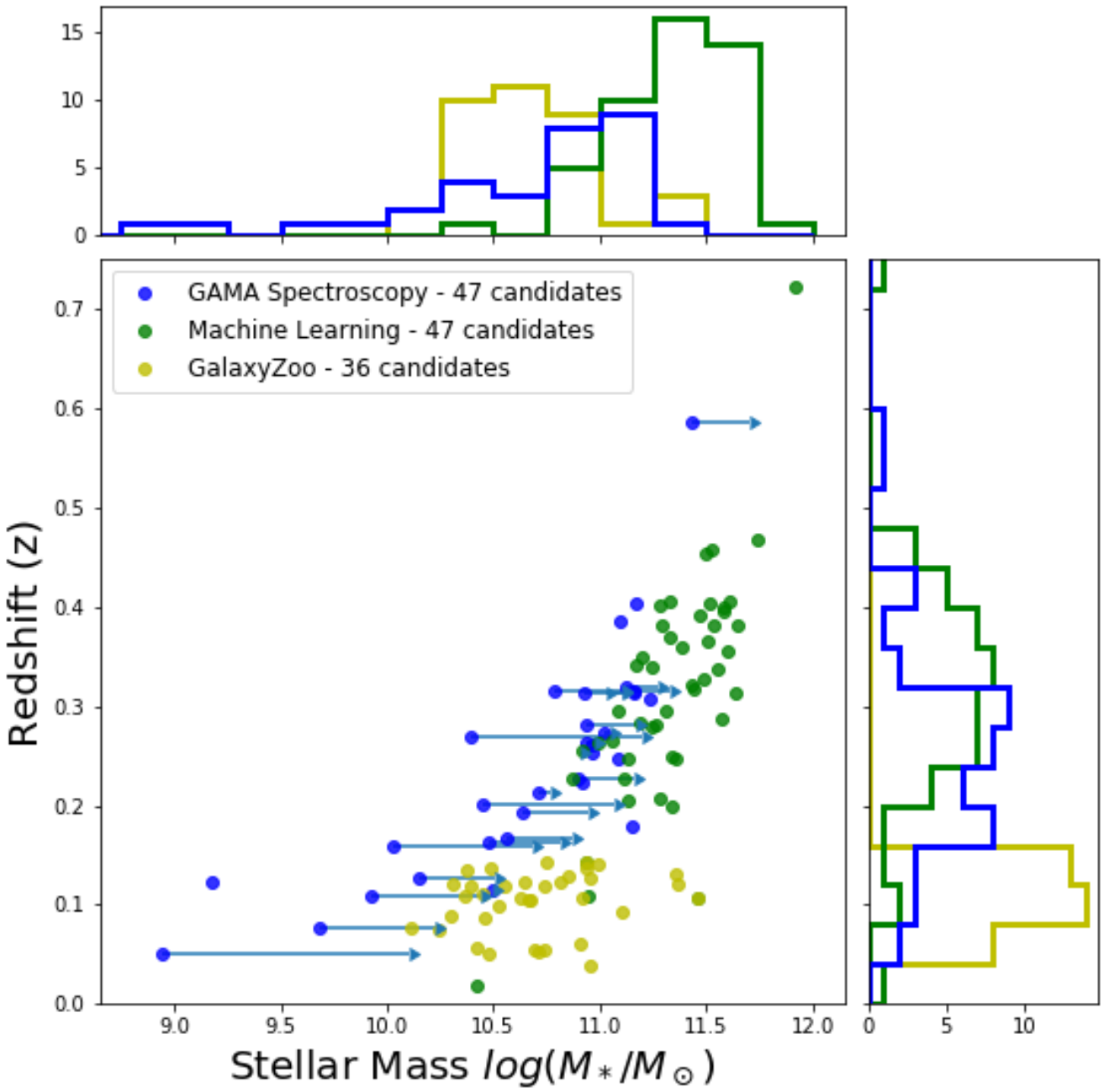

Figure 12. The data presented here is the same as in Figure 10 with additional error bars introduced to represent the estimated maximum stellar mass that could be enclosed by an Einstein radius of $\theta_E = 1$ arcsecond (corresponding to the aperture-size of GAMA spectroscopic fibers). Several candidates identified by the other two methods have mass that exceed this maximum mass at the given redshift.

4.3. *Overlapping Candidates*

The two candidates (G136604 and G124486) common to both LinKS machine learning and GalaxyZoo citizen science, fall within the overlap of the parameter space occupied by the two methods' samples in terms of stellar mass and redshift, as shown in Figure 10. Their masses are (G136604) $2.866\times10^{11}(M_*/M_\odot)$ and (G124486) $8.541\times10^{10}(M_*/M_\odot)$ and redshifts z = 0.106 and z = 0.1435. The "Lens or arc" score given to these candidates in GalaxyZoo citizen science

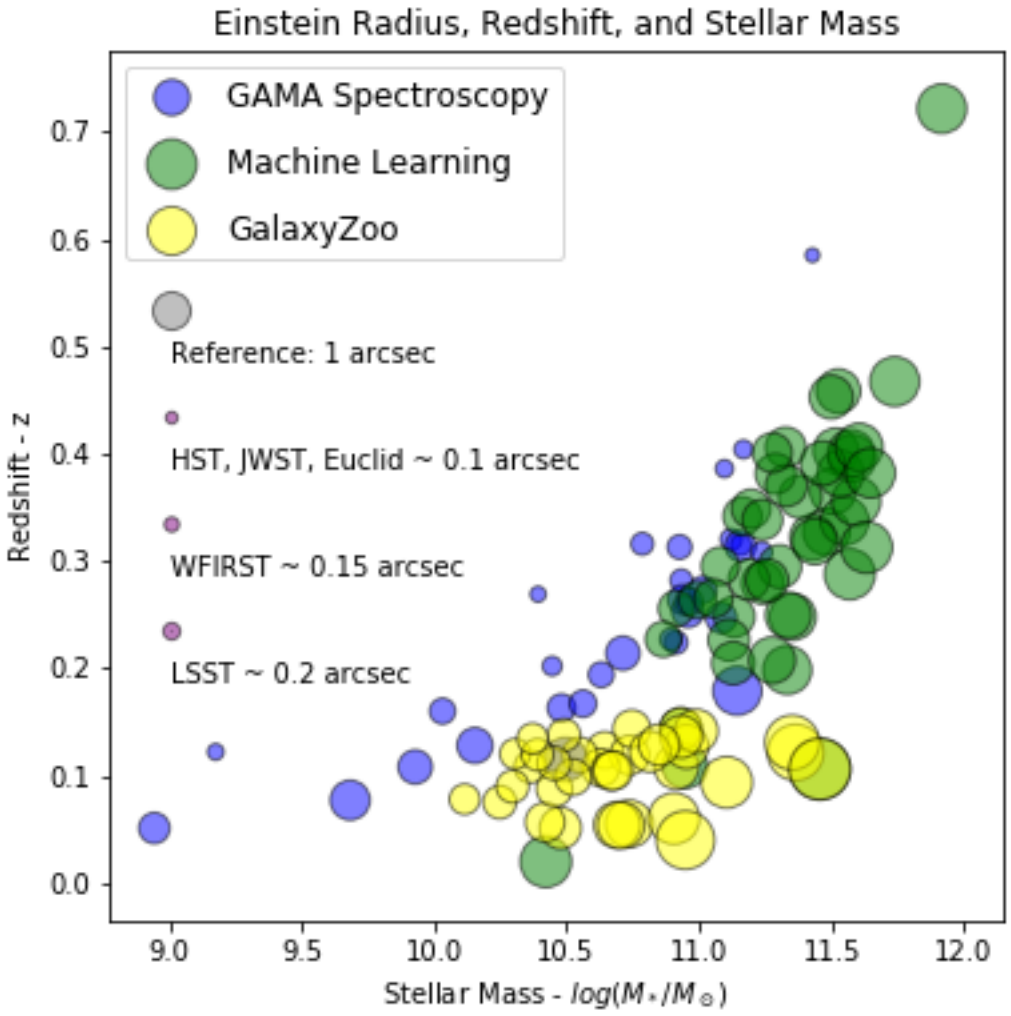

Figure 13. The data presented here is the same as in Figure 10 with marker-size corresponding to Einstein radius. The largest of Einstein radii tend to be at higher mass and lower redshift. The gray reference marker indicates the benchmark of $\theta_E = 1$ arcsecond (corresponding to the aperture-size of GAMA spectroscopic fibers). Next generation surveys (JWST, Euclid, WFIRST, LSST) will have optical resolutions comparable to HST, on the order of 0.1-0.2 arcseconds. In theory, under the right conditions, these surveys should be able to resolve even the smallest Einstein radii ($\theta_E = 0.141$ arcsec) considered in this survey.

Table 1. Overlap of LinKS Machine Learning and GalaxyZoo citizen science Samples.

GAMAID	RA	DEC	$(M_*/M_\odot)$	z	θ_E (arcsec)	ML Score	GZ Score
G136604	175.87	-1.74	2.87×10^{11}	0.106	2.63	58	31.65%
G124486	179.73	-2.52	8.54×10^{10}	0.144	1.24	28	42.62%

(G136604: 31.6% and G124486: 42.6%) and the visual inspection scores from LinKS machine learning (G136604: 58 and G124486: 28) make these two of the most promising candidates.

5. SELECTION EFFECTS

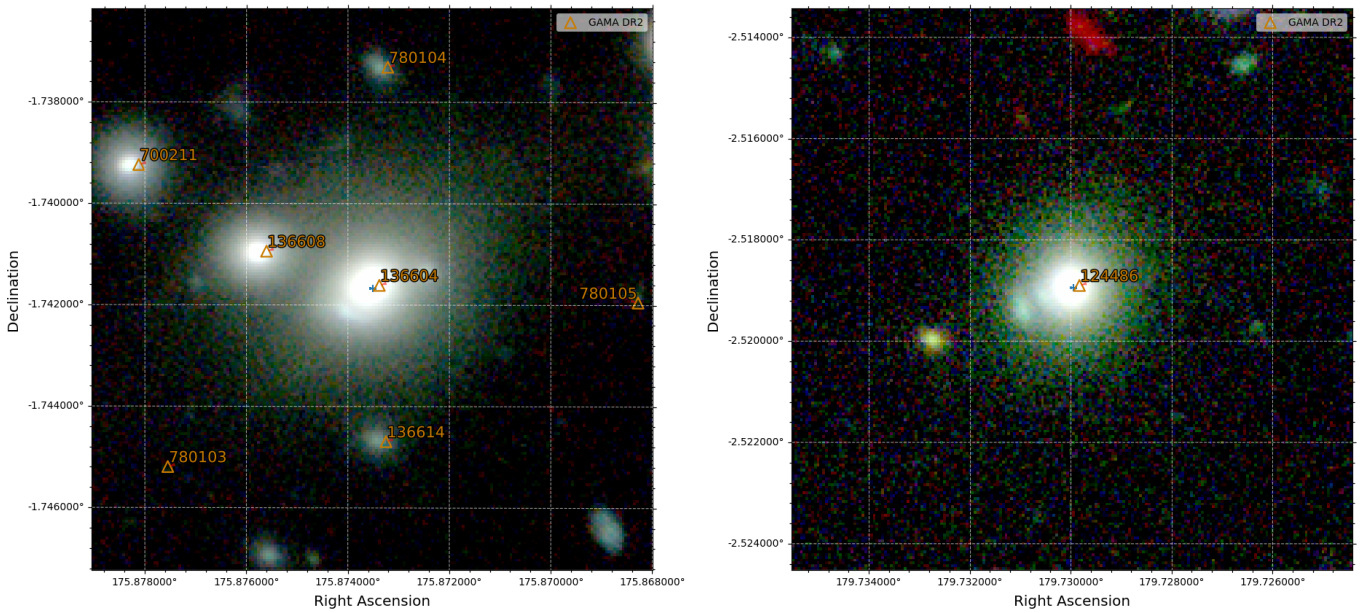

Figure 14. G136604 and G124486, the two candidates identified by both LinKS machine learning and GalaxyZoo citizen science. NOTE SCORES: score given to these candidates in GalaxyZoo citizen science (G136604: 31.6% and G124486: 42.6%) and the visual inspection scores from LinKS machine learning (G136604: 58 and G124486: 28).

GAMA spectroscopy candidates are selected from a parent subsample of spectroscopic targets in the equatorial regions of GAMA DR3 with spectral template matches of greater than 90% confidence to one of three passive galaxy templates in the autoz algorithm. Stellar masses and redshifts are taken from the GAMA MagPhys catalog, and the resulting sample of passive galaxies in GAMA is taken to be the "parent sample" for the GAMA spectroscopy lens candidate sample. Kolmogrov-Smirnoff tests between the lens candidate sample and the passive galaxy sample reveal K-S metrics and p-values of 0.0845 and 0.877 in terms of redshift and 0.340 and $2.433 * 10^{-5}$ in terms of stellar mass.

The LinKS sample (**?**) of machine learning candidates, like its training sample, was selected using color-magnitude cuts modified from the SDSS-LRG (Large Red Galaxy) (!!! Eisenstein-2001, Petrillo et al. (2017), **?**) low-z selection criteria. The parent sample for candidates selected within the GAMA equatorial regions includes all galaxies within those regions that satisfy the LRG criteria. Color-magnitude selection includes the following:

$$r < 20$$

$$c_{perp} < 0.2$$

$$r < 14 + \frac{c_{par}}{0.3}$$

where

$$c_{par} = 0.7(g - r) + 1.2[(r - i) - 0.18)]$$

$$c_{perp} = (r - i) - \frac{g - r}{4.0} - 0.18$$

AB magnitudes are taken from GAMA Lambdar SDSS $g-$, $r-$, and $i-$ catalogs. Stellar mass and redshift are taken from GAMA MagPhys. K-S tests between the LinKS machine learning lens candidate sample and the GAMA equatorial LRG sample reveal K-S metrics and p-values of 0.329 and $5.23*10^{-05}$ in terms of redshift and statistic=0.663 and $4.57 * 10^{-19}$ in terms of stellar mass.

GalaxyZoo selects only objects whose redshift $z < 0.15$, so the parent sample for the GalaxyZoo lens candidate sample contains all galaxies within the GAMA equatorial fields below that redshift upper limit. Redshifts and stellar masses are taken again from the GAMA MagPhys catalog, and K-S tests of redshift and stellar mass yield (K-S metric, p-value) of (0.0997, 0.849) and $(0.621, 4.92 * 10^{-13})$ respectively.

Conclusion alpha/omega: lensing searches of any kind prefer higher mass. GZ and GAMA spectroscopy no redshift bias evident. ML do have a redshift preference.

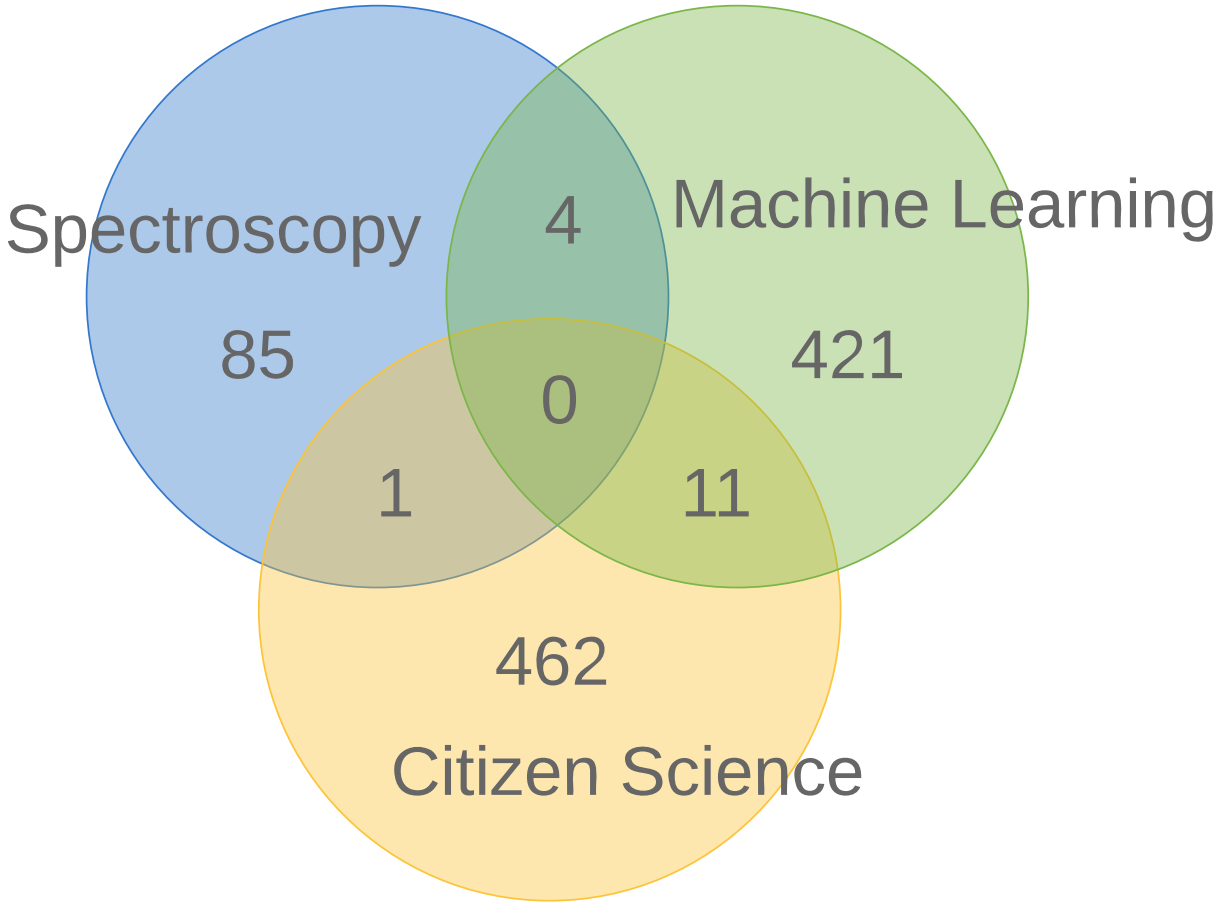

Figure 15. Venn diagram showing the number of lens candidates identified by each of the three methods with more lenient cuts to both GalaxyZoo citizen science and LinKS machine learning. Candidates with "Lens or arc" scores above 20% and LinKS machine learning candidates with lens scores greater than 0 are included in this selection. Overlapping regions indicate the number of lens candidates identified by both (or all three) candidates.

6. DISCUSSION

6.1. *Alternate Cuts*

The final cuts were intended to ensure a comparable and reliable catalog of lens candidates for each method analyzed. The numbers reflected in our final catalogs will vary if considered under different cuts, so we also examined the overlap considering a more relaxed cut that included all GalaxyZoo candidates with lens scores greater than 20% and all LinKS machine learning candidates with scores greater than 0. Figure 15 shows that this cut improves overlap to a small extent, but it introduces a significant increase in false-positives and unreliable candidates, which we considered to outweigh the benefits of the improvement to overlap for the purposes of this study. The overlaps that we see in the more relaxed cuts do appear in the expected parameter space, with masses and redshifts comparable to the two overlap candidates that appear in our final catalogs.

6.2. *LinKS machine Learning Training Set*

Machine learning is an effective method for identifying image features similar to the training set utilized. Its effectiveness is then constrained inherently by the scope of its training set. The catalog analyzed here from Petrillo et al. (2018) used simulated images resembling SLACS lenses as their training set, and the candidates it identified are characteristically similar in terms of stellar mass and redshift to those identified by SLACS spectroscopy. With a training sample volumetrically skewed towards massive elliptical galaxies (the early-type galaxies sample in KiDS), the resulting identified lenses are equally biased toward higher masses.

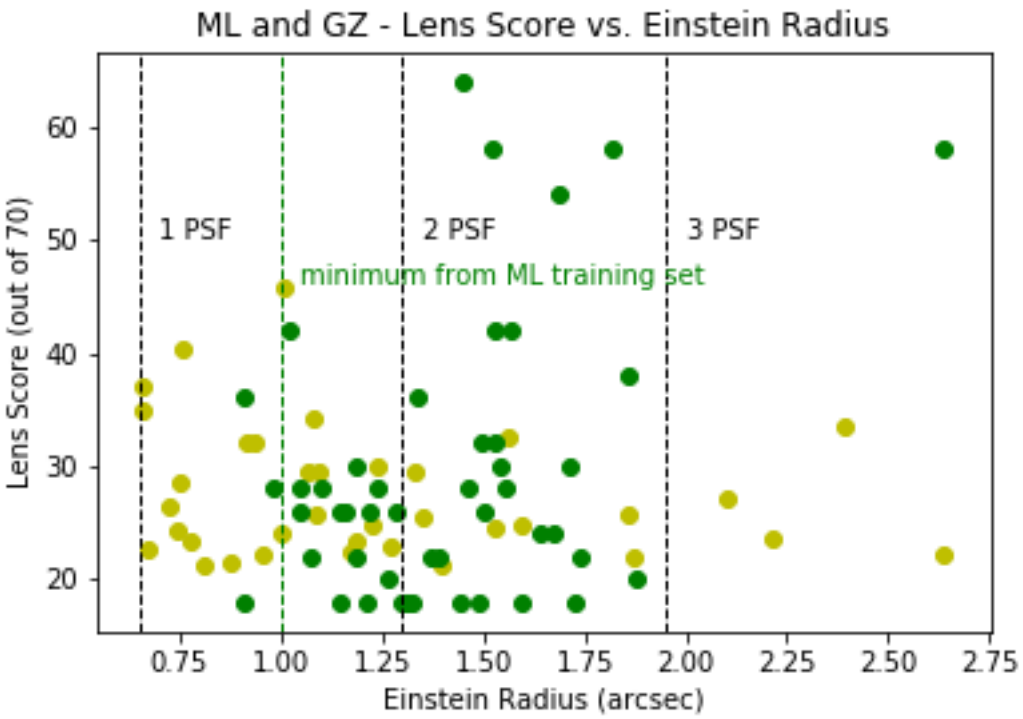

Figure 16. Caption

6.3. *LinKS machine Learning Training set*

Figure and discussion of figure.

6.4. *Maximum Stellar Mass in GAMA Spectroscopic Identification*

Lens candidate identification through any spectroscopic method requires sufficient flux from the background galaxy in order to obtain a second spectral match. For lensing systems whose Einstein radius exceeds the radius of the instrument's aperture, the probability of detection goes down significantly (!!!!Sonnenfeld-2015, Arneson et al. (2012)). For lensing systems with known lens and source redshifts, there is then a soft constraint on the maximum total mass that will contribute to an Einstein radius that will fit within the instrument's aperture. Taking into account GAMA spectroscopy's 1″-radius aperture and assuming $f_{DM} = 61\%$, the estimates for this upper limit to stellar mass are calculated and shown as error-bars in Figure 12. Several candidates from the other two methods have stellar masses exceeding this upper limit at similar redshifts. This ensures that GAMA spectroscopy will have little chance of observing enough flux from the background galaxy to acquire the second redshift match required for candidate identification.

6.5. *Low-Mass Lensing Galaxies*

GalaxyZoo citizen science and GAMA spectroscopy found an encouraging number of lenses at lower masses than those identified through the LinKS machine learning method considered here, as well as most previous lens studies that focused on galaxies fitting the description of SDSS LRGs (!!! Eisenstein-2001). These lenses could potentially be analyzed in order to study the structure of galaxies and their dark matter content in this lower range of galaxy mass. However, each arc from GalaxyZoo will need to be confirmed spectroscopically before modeling these as lensing systems, and more samples are needed in order to study this parameter space with meaningful results.

6.6. *Candidates and LRG Color-Magnitude Selection*

The color-magnitude selection criteria for SDSS-LRGs detailed in Section 5 were applied to the final candidate samples of the LinKS machine learning and GalaxyZoo citizen science methods. Only 6 of the 36 GalaxyZoo candidates

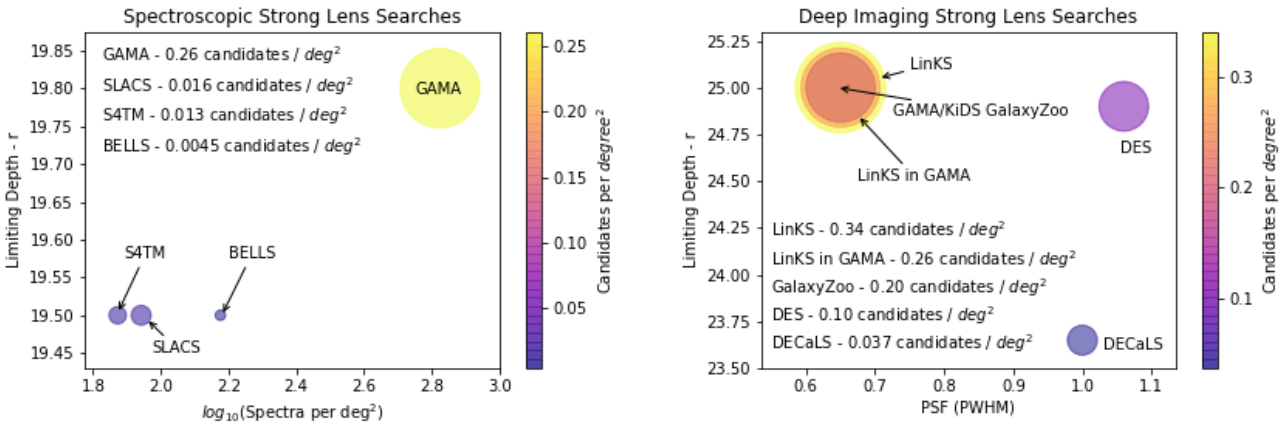

Figure 17. A comparison between the different identifications of strong galaxy-galaxy lenses in different surveys, using blended spectroscopy (left) and deep imaging (right). The left figure shows SLACS (Bolton et al. 2006), S4TM (Shu et al. 2018) and BELLS (Brownstein et al. 2012) spectroscopic searches compared to the GAMA spectroscopy candidates selected in this work from (Holwerda et al. 2015). The right figure shows the LinKS survey from **?** and the candidates presented in this paper from GAMA/KiDS GalaxyZoo citizen science, compared with deep imaging searches in DES (Jacobs et al. 2019) and DECaLS (Huang et al. 2019).

Table 2. Strong lenses with archival Hubble data available from the Hubble Legacy Archive.

GAMAID	RA	DEC	Method
G136604	175.87349	-1.74167	ML & GZ
G204703	139.07321	-0.40157	ML
G3882191	133.69397	-1.36032	ML
G593852	218.0782	-0.03958	GZ

and 7 of the 47 LinKS candidates passed this selection, indicating that the more strong lenses are to be found by broadening the search and training sets beyond the assumption of LRG dominance (!!! Li-2020).

6.7. *Other Lens Searches and Future Efforts*

Similar efforts, mostly machine learning, have found strong lens candidates in deep imaging surveys (e.g., Speagle et al. 2019; Huang et al. 2019; Jacobs et al. 2019, in HSC, DECaLS and DES respectively). Figure 17 shows the numbers of identified lenses per unit of sky against the survey characteristics. The majority of theses studies aimed for a clean (reliable but incomplete) rather than complete sample of galaxy-galaxy lenses. Our results show that the combination of methods implies a much higher sky density of lenses in a given survey. Key for spectroscopic survey identification is completeness, a key driver of GAMA survey (Driver et al. 2009; Robotham et al. 2010; Baldry et al. 2011), and an automated redshift finder (Baldry et al. 2014). For imaging surveys, the key drivers are spatial resolution (subarcsecond seeing) and survey depth. The on-sky density of strong lenses is critical if one wants to estimate, for example, the rates of strongly lensed events such as supernovae (Holwerda et al. *in prep.*).

The Hubble Legacy Archive (HLA) (Whitmore et al. 2016) contains imaging information on four of the lensing candidates presented here in Table 2. Figure 18 shows two of these examples. G136604 was identified in both the LinKS machine learning and GalaxyZoo citizen science selections (shown also in Figure 14, left) and was a known strong lens from the SLACS survey (Bolton et al. 2008; Auger et al. 2010; Barnabè et al. 2011; Bolton et al. 2012; Czoske et al. 2012; Shu et al. 2015). The second example, G204703, is part of a cluster, and the arc is partially the result of cluster strong lensing (Zitrin & Broadhurst 2016; Zitrin 2017; Dessauges-Zavadsky et al. 2017; Newman et al. 2018). One of the GalaxyZoo identifications, G593852, is in the HLA, but the arc is faint in the Hubble single filter image (Figure 18). These images illustrate that all the selection methods find valid strong lenses and show that Hubble images on these would validate their nature and make detailed lensing models possible.

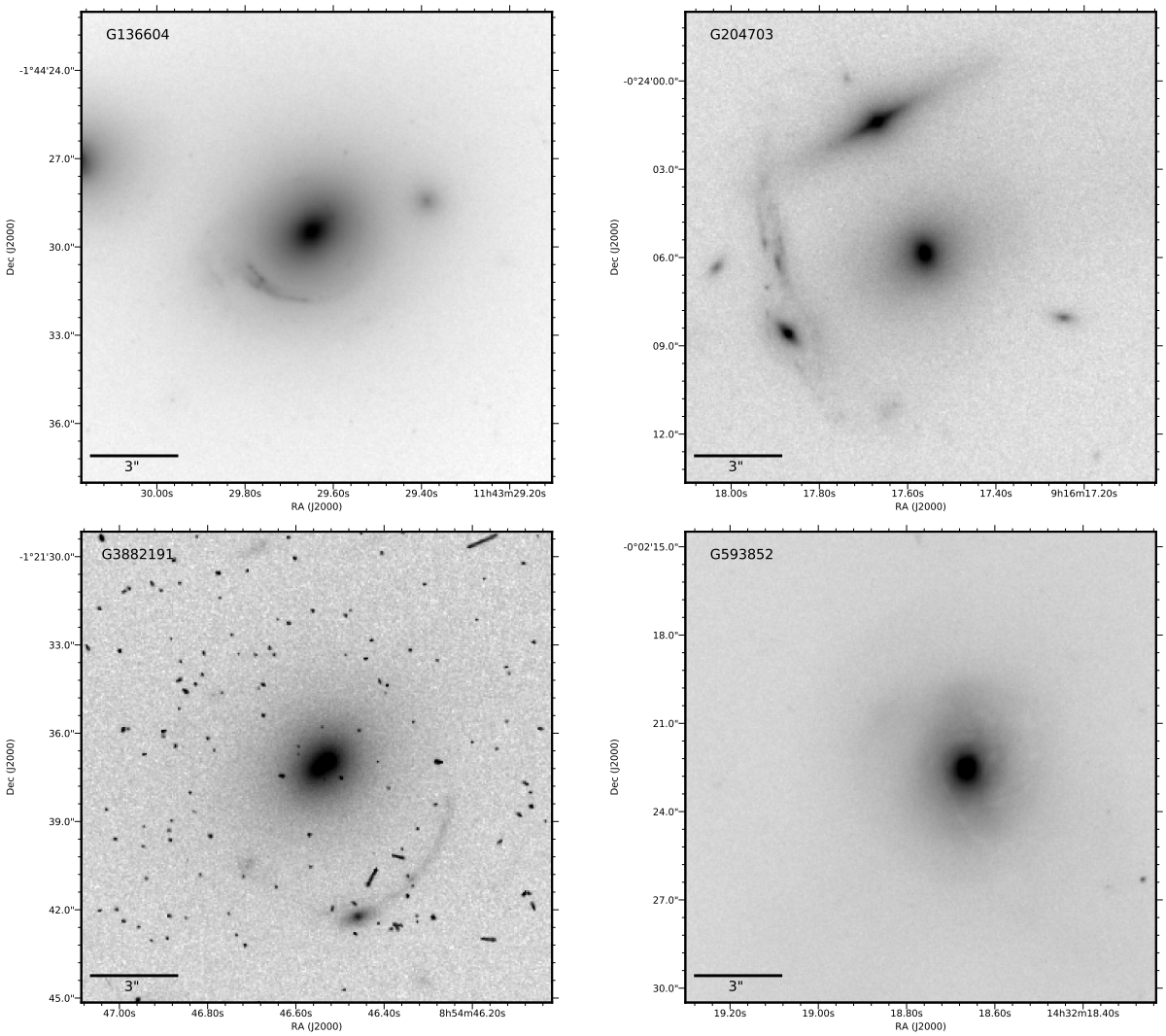

Figure 18. Examples of lensing candidates found in the Hubble Legacy Archive (HLA). Grayscale image in F814W, except G593852, which is in F625W. G136604 was identified earlier in SLACS, by LinKS machine learning and GalaxyZoo citizen science. The arc next to G204703 may be due to cluster lensing. G3882191 was identified in SLACS previously, and G3882191 is the faint arc identified by GalaxyZoo.

With improved spatial resolution for wide-field imaging (WFIRST and EUCLID), the machine learning and citizen science identification will overlap more in mass and redshift with the spectroscopic identifications of strong lenses. Wide-field integral field spectroscopy (e.g. SAMI, MUSE, and 4MOST WAVES wide surveys) could potentially identify strong lenses from a mix of spectroscopic and imaging information (curved arc in the data-cube).

For future identification of galaxy-galaxy lenses (e.g. LSST or WFIRST imaging), a hybrid approach between citizen science and machine learning (see Beck et al. 2018) could result in a more complete and reliable yield of strong lensing candidates. This is in our view a better approach than to try to validate galaxy-galaxy lenses using different methods. Alternatively, an entirely new selection technique could result in a selection of similar completeness as the three presented here.

7. CONCLUSIONS

Our analysis of the data generated by the three methods leads us to the following conclusions regarding the biases and advantages of the methods as well as the relation of each to the others:

- The three specific methods analysed here are ineffective means of vetting candidate samples obtained by either of the other two methods due to the lack of overlap between candidate properties, which we illustrate in Figures 8 and 10.
- The differences in candidate properties arise primarily from selection functions inherent to the parent sample selections and procedures of each method; specifically:
  - Blended spectra identifies only those candidate galaxies whose lens features contribute significant flux within the radius of the fiber aperture collecting the spectrum. GAMA's depth and completeness extend candidate selection to a lower mass range. A wider aperture or integral field spectroscopy (e.g. SAMI or MUSE) would allow the possibility of identifying lower redshift or more massive galaxies.
  - Machine learning finds candidates with similar features to its training sets, i.e. well-separated lens and arc. This limitation can be improved upon with higher-resolution images and a wider variation in training sets, including lens galaxies that do not conform to LRG characteristics.
  - GalaxyZoo's upper threshold on redshift limits its range of applicability, and the wide focus of its classification stage introduces significant challenges to candidate quality assessment. Higher-resolution images and a higher redshift cutoff together would allow for the inclusion of farther galaxies, e.g. for WFIRST, LSST, or Euclid citizen science efforts.
- Machine learning has the promise to be the most efficient automated lens identification technique, and substantial effort must be made to improve these algorithms ahead of the next generation of galaxy surveys.
- In the meantime, other methods – including blended spectra and citizen science – remain useful for extending and diversifying the catalog of lens candidates available for study and for their application in the training of machine learning algorithms.

Strong gravitational lenses offer a unique laboratory to be used in cosmology measures and the next level of accuracy in estimates of dark matter distribution and substructure. The much greater samples needed (orders of magnitude higher than the current number of identified lenses) require automated identification. Using a combined approach, a more complete census of these rare objects can be achieved for the next generation of imaging surveys (e.g. WFIRST, Euclid, and LSST). Future large telescopes (GMT/ELT/TMT) could follow-up the higher redshift or lower mass lenses, and the WEAVE and 4MOST instruments are set to select or confirm many lenses spectroscopically.

ACKNOWLEDGEMENTS

S. Knabel acknowledges the support of the Summer Research Opportunity Program (SROP) and the Undergraduate Research Grant (URG) by the University of Louisville's Office of the Executive Vice President for Research and Innovation (EVPRI). The material is based upon work supported by NASA Kentucky under NASA award No: NNX15AR69H (R. Steele).

8. APPENDIX

Table 3. GalaxyZoo Citizen Science Lens Candidates

GAMA ID	Stellar Mass $\log(M_*/M_\odot)$	Redshift (z)	Lens Score	RA	Dec
7104	10.24748	0.07510	33.333%	175.71213	0.83228
16199	10.25575	0.12450	32.975%	217.85542	0.70541
32675	10.08493	0.14600	52.717%	185.70777	-1.1103
39718	9.95173	0.08090	38.309%	177.9385	-0.71802
40666	10.01662	0.10670	36.016%	182.46693	-0.78528
40957	9.34459	0.12430	33.425%	183.73733	-0.69189
55245	11.10517	0.09360	31.405%	181.07958	-0.31553
70022	10.90558	0.05990	36.811%	178.02218	0.07392
70282	10.62900	0.10740	65.535%	179.40308	0.12562
70376	10.19396	0.13080	31.360%	179.62517	0.05585

Table 3. GalaxyZoo Citizen Science Lens Candidates

GAMA ID	Stellar Mass $\log(M_*/M_\odot)$	Redshift (z)	Lens Score	RA	Dec
84050	10.73807	0.11900	36.576%	175.79849	0.47814
93310	10.49052	0.13770	57.514%	219.92276	0.50731
93803	10.94910	0.03980	47.772%	222.48917	0.55835
106562	10.95352	0.12680	36.388%	216.62566	0.84498
124486	10.93151	0.14350	42.619%	179.72998	-2.51919
136581	9.67228	0.08530	38.876%	175.67082	-1.66467
136604	11.45728	0.10600	31.645%	175.87349	-1.74167
144068	10.37585	0.14460	33.041%	178.83194	-1.40894
164403	10.29601	0.08980	40.659%	177.41987	-2.72815
164479	10.07335	0.09930	35.680%	177.6572	-2.81587
165259	10.00432	0.10180	33.577%	180.44234	-2.82167
170898	11.36530	0.12150	33.610%	176.46563	-2.33643
171055	9.56902	0.13140	30.765%	176.8102	-2.2989
184275	10.64454	0.12370	31.726%	175.91698	-1.44119
185451	10.91498	0.10790	30.298%	180.28326	-1.61006
196837	10.67578	0.10460	48.734%	132.90975	-0.69973
197611	10.00518	0.11630	31.935%	136.03367	-0.72014
202397	8.77041	0.05220	34.729%	129.44792	-0.24408
216186	10.01828	0.14670	45.970%	137.06817	0.53355
218733	10.99003	0.14150	41.959%	140.29763	0.88594
229499	8.20952	0.04500	45.218%	223.08137	1.0355
238271	10.84991	0.12870	33.169%	213.72842	1.57878
267558	8.93656	0.13580	33.474%	222.88792	2.70549
272460	9.66876	0.13350	32.867%	179.4985	1.42932
287627	10.37144	0.13440	32.279%	174.1965	1.69352
289994	10.26670	0.11380	33.261%	184.23553	1.85313
299118	10.11093	0.14600	55.961%	223.34617	1.14187
320551	10.11494	0.07790	52.964%	218.67851	1.78336
324764	10.66717	0.10440	42.276%	137.20387	1.72633
342161	9.75884	0.12850	39.017%	214.4815	2.29663
342699	10.45408	0.08760	45.709%	216.90174	2.1325
342874	9.74044	0.14040	31.743%	217.70954	2.18624
363319	10.52414	0.09850	45.753%	218.85395	2.56676
363983	10.35218	0.14440	40.001%	222.27717	2.43775
371601	9.79505	0.06070	31.988%	132.01727	1.03236
372045	10.39041	0.11940	37.830%	133.97321	0.9832
418788	10.74648	0.14360	34.306%	137.69141	2.74717
422113	10.30535	0.12020	49.958%	129.41517	2.59516
422228	10.45286	0.11150	30.214%	129.93613	2.59097
460645	10.55011	0.11920	30.708%	213.23176	-1.721
485873	10.69090	0.05390	34.946%	217.75015	-1.80042
491505	9.21564	0.07610	42.970%	212.1493	-1.51127
511867	10.73711	0.05500	35.223%	216.38846	-1.11396
521819	9.63629	0.07920	49.689%	131.36708	2.91472
543556	9.67560	0.08710	56.973%	211.99696	-0.99252
543671	10.08920	0.14080	40.568%	212.42117	-0.89741
560204	9.92947	0.08440	38.018%	179.65787	-0.48421
567899	10.15473	0.13860	32.992%	213.60875	-0.52841

Table 3. GalaxyZoo Citizen Science Lens Candidates

GAMA ID	Stellar Mass $\log(M_*/M_\odot)$	Redshift (z)	Lens Score	RA	Dec
568545	10.47683	0.05100	35.501%	215.4957	-0.59009
568546	8.82640	0.05120	61.258%	215.49492	-0.58888
570151	9.67988	0.13970	37.087%	222.24417	-0.54052
573840	10.18070	0.13540	31.521%	130.33075	-0.20663
574423	10.70578	0.05360	46.434%	135.75994	-0.20038
586565	9.86587	0.10830	35.433%	185.45096	-0.00661
593691	10.36418	0.10810	34.844%	217.50766	-0.12318
593852	11.35238	0.13080	38.632%	218.0782	-0.03958
594681	9.61151	0.14610	41.182%	221.11008	-0.05868
600421	10.41847	0.05650	42.019%	135.49058	0.28417
600679	9.57206	0.10100	41.929%	136.8274	0.25166
771379	9.25358	0.13700	35.802%	219.9235	0.50872
3578853	10.81538	0.12210	31.946%	130.98196	-1.62032
3593943	10.33021	0.13790	54.567%	139.74883	-1.87208
3599976	9.51957	0.11030	30.950%	129.38913	-1.10436
3610455	10.08565	0.12720	33.082%	135.09329	-1.21204
3632594	10.93313	0.13620	32.667%	138.25246	-0.95549
3909064	9.65485	0.07800	42.051%	136.9855	-1.14841

REFERENCES

Arneson, R. A., Brownstein, J. R., & Bolton, A. S. 2012, ApJ, 753, 4

Auger, M. W., Treu, T., Bolton, A. S., et al. 2009a, ApJ, 705, 1099

—. 2009b, ApJ, 705, 1099

—. 2010, ApJ, 724, 511

Baldry, I. K., Driver, S. P., Loveday, J., et al. 2011, ArXiv e-prints

Baldry, I. K., Alpaslan, M., Bauer, A. E., et al. 2014, MNRAS, 441, 2440

Baldry, I. K., Liske, J., Brown, M. J. I., et al. 2018, MNRAS, 474, 3875

Barnabè, M., Czoske, O., Koopmans, L. V. E., Treu, T., & Bolton, A. S. 2011, MNRAS, 415, 2215

Beck, M. R., Scarlata, C., Fortson, L. F., et al. 2018, ArXiv e-prints

Bolton, A. S., Burles, S., Koopmans, L. V. E., Treu, T., & Moustakas, L. A. 2006, ApJ, 638, 703

Bolton, A. S., Burles, S., Schlegel, D. J., Eisenstein, D. J., & Brinkmann, J. 2004, AJ, 127, 1860

Bolton, A. S., Treu, T., Koopmans, L. V. E., et al. 2008, ApJ, 684, 248

Bolton, A. S., Schlegel, D. J., Aubourg, E., et al. 2012, ArXiv e-prints

Brownstein, J. R., Bolton, A. S., Schlegel, D. J., et al. 2012, ApJ, 744, 41

Chan, J. H. H., Suyu, S. H., More, A., et al. 2016, ApJ, 832, 135

Chen, G. C.-F., Fassnacht, C. D., Suyu, S. H., et al. 2019, MNRAS

Cluver, M. E., Jarrett, T. H., Hopkins, A. M., et al. 2014, ApJ, 782, 90

Collett, T. E., Oldham, L. J., Smith, R. J., et al. 2018, ArXiv e-prints

Collier, W. P., Smith, R. J., & Lucey, J. R. 2018a, MNRAS, 473, 1103

—. 2018b, ArXiv e-prints

Cyr-Racine, F.-Y., Keeton, C. R., & Moustakas, L. A. 2018, ArXiv e-prints

Czoske, O., Barnabè, M., Koopmans, L. V. E., Treu, T., & Bolton, A. S. 2012, MNRAS, 419, 656

de Jong, J. T. A., Verdoes Kleijn, G. A., Kuijken, K. H., & Valentijn, E. A. 2013, Experimental Astronomy, 35, 25

de Jong, J. T. A., Verdoes Kleijn, G. A., Boxhoorn, D. R., et al. 2015, A&A, 582, A62

de Jong, J. T. A., Kleijn, G. A. V., Erben, T., et al. 2017, A&A, 604, A134

De Lucia, G., Springel, V., White, S. D. M., Croton, D., & Kauffmann, G. 2006, MNRAS, 366, 499

Dessauges-Zavadsky, M., Zamojski, M., Rujopakarn, W., et al. 2017, A&A, 605, A81
Driver, S. P., Norberg, P., Baldry, I. K., et al. 2009, Astronomy and Geophysics, 50, 050000
Driver, S. P., Hill, D. T., Kelvin, L. S., et al. 2011, MNRAS, 413, 971
Gavazzi, R., Treu, T., Koopmans, L. V. E., et al. 2008, ApJ, 677, 1046
Gavazzi, R., Treu, T., Rhodes, J. D., et al. 2007, ApJ, 667, 176
Hilbert, S., White, S. D. M., Hartlap, J., & Schneider, P. 2008, MNRAS, 386, 1845
Holwerda, B. W., Baldry, I. K., Alpaslan, M., et al. 2015, MNRAS, 449, 4277
Holwerda, B. W., Kelvin, L., Baldry, I., et al. 2019, AJ, 158, 103
Hopkins, A. M. 2018, ArXiv e-prints
Huang, X., Domingo, M., Pilon, A., et al. 2019, arXiv e-prints
Jacobs, C., Collett, T., Glazebrook, K., et al. 2019, arXiv e-prints
Koopmans, L. V. E., Treu, T., Bolton, A. S., Burles, S., & Moustakas, L. A. 2006, ApJ, 649, 599
Kuijken, K., Heymans, C., Dvornik, A., et al. 2019, arXiv e-prints
Lintott, C. J., Schawinski, K., Slosar, A., et al. 2008, MNRAS, 389, 1179
Liske, J., Baldry, I. K., Driver, S. P., et al. 2015, MNRAS, 452, 2087
Newman, A. B., Belli, S., Ellis, R. S., & Patel, S. G. 2018, ApJ, 862, 125
Petrillo, C. E., Tortora, C., Chatterjee, S., et al. 2017, MNRAS, 472, 1129
—. 2018
Riess, A. G., Macri, L., Casertano, S., et al. 2011, ApJ, 730, 119
Robotham, A., Driver, S. P., Norberg, P., et al. 2010, PASA, 27, 76
Shu, Y., Bolton, A. S., Mao, S., et al. 2018, ApJ, 864, 91
Shu, Y., Bolton, A. S., Brownstein, J. R., et al. 2014, ArXiv e-prints
—. 2015, ApJ, 803, 71
Shu, Y., Brownstein, J. R., Bolton, A. S., et al. 2017
Sonnenfeld, A., Treu, T., Marshall, P. J., et al. 2015, ApJ, 800, 94
Speagle, J. S., Leauthaud, A., Huang, S., et al. 2019, arXiv e-prints
Tortora, C., Koopmans, L. V. E., & Napolitano, N. R. 2017, ArXiv e-prints
Treu, T., Gavazzi, R., Gorecki, A., et al. 2009, ApJ, 690, 670
Treu, T., Koopmans, L. V., Bolton, A. S., Burles, S., & Moustakas, L. A. 2006, ApJ, 640, 662
Verlinde, E. P. 2016, ArXiv e-prints
Whitmore, B. C., Allam, S. S., Budavari, T., et al. 2016, ArXiv e-prints
Wright, A. H., Driver, S. P., & Robotham, A. S. G. 2018, MNRAS
Zitrin, A. 2017, ApJ, 834, 45
Zitrin, A., & Broadhurst, T. 2016, ApJ, 833, 25